

Fabrication of Porous Metals via Selective Phase Dissolution of an Al–Cu Alloy

by

Juan Carlos Vargas Martinez

A thesis submitted in partial fulfillment of the requirements for the degree of

MASTER OF SCIENCE
in
MECHANICAL ENGINEERING
(Materials and Manufacturing)

UNIVERSITY OF PUERTO RICO
MAYAGÜEZ CAMPUS
2018

O. Marcelo Suárez, Ph.D.
President, Graduate Committee

Date

Arturo Hernández, Ph.D.
Member, Graduate Committee

Date

Néstor Pérez, Ph.D.
Member, Graduate Committee

Date

Pedro Quintero, Ph.D.
Member, Graduate Committee

Date

Néstor Pérez, Ph.D.
Director of Mech. Eng. Department

Date

Nelson Cardona, Ph.D.
Representative of Graduate Studies

Date

ABSTRACT

Through free corrosion in sodium hydroxide, a new porous material was successfully fabricated by removing a single phase of the aluminum-copper alloy. This selective phase dissolution was performed for the eutectic composition of the aluminum-copper binary system and additionally for two hypereutectic compositions. The porosity of the material depends on the microstructure formed in the solidification process. For this, several solidification methods were analyzed in order to define the most convenient in terms of uniformity and refinement in the pore and ligament sizes. The concentration of the solution was determined by observing the effectiveness of the process during and after the corrosion, when the 10% v/v aqueous solution of sodium hydroxide was used better results were observed. The porosity was calculated after the selective dissolution through analysis of images obtained from a scanning electron microscope. In addition, the average pore and ligament size was measured for each composition. Finally, the effectiveness of the process was verified using x-ray diffraction, which showed that under the proposed methodology there was complete removal of one of the phases of the alloy.

RESUMEN

Mediante la corrosión libre en hidróxido de sodio, se fabricó de manera exitosa un nuevo material poroso a través de la eliminación de una fase de una aleación de aluminio y cobre. Esta disolución selectiva de fase se realizó para la composición eutéctica del sistema binario de aluminio-cobre y adicionalmente para dos composiciones hipereutécticas. La porosidad del material depende de la microestructura formada en el proceso de solidificación. Para esto, se analizaron varios métodos de solidificación con el fin de definir el más conveniente en términos de uniformidad y refinamiento en los tamaños de poro y ligamento. La concentración de la solución se determinó observando la efectividad del proceso durante y después de la corrosión. Cuando se usaron soluciones acuosas al 10% v/v de hidróxido sódico, se observaron mejores resultados. La porosidad se calculó después de la disolución selectiva a través del análisis de imágenes obtenidas a partir de un microscopio electrónico de barrido. Además, se midió el tamaño medio de poro y ligamento para cada composición. Finalmente, se verificó la efectividad del proceso usando difracción de rayos X, lo que demostró que bajo la metodología propuesta se eliminó por completo una de las fases de la aleación.

Copyright © by
Juan Carlos Vargas Martinez
2018

To God for giving me the strength

ACKNOWLEDGMENTS

I am very thankful with my advisor Oscar Marcelo Suárez for his direction and support in my research. Also to the graduate committee and the graduate studies representative.

Thanks to my friends of the research lab: Boris Rentería, Carlos Rivera, David Florián, Andres Calle, Hildéliz Soto, Amarillys Avilés, Sujeily Soto, Wesley Cuadrado, Johnny Lopez, Manny De Jesús, Ulises Barajas. In addition, my gratitude goes to the undergraduate students that make part of this project: Abel Urbán, John Estela, Aleysha Vargas, Keishlyann Báez, Johnattan Díaz and Kenneth Silva.

I would like to thank to Margie Guerrero for her support in the SEM images, as well as to Dr. Frank Mendoza (IFN-UPR-Rio Piedras) and Dr. Wilfredo Otaño (University of Puerto Rico – Cayey) for their assistance.

Thanks to my family for their support in this path of my life.

Finally, this work was partly supported by the National Science Foundation under Grant No. 1345156 (CREST program).

TABLE OF CONTENTS

Abstract	ii
Resumen.....	iii
Acknowledgments	v
Table of contents	vii
List of figures.....	ix
List of tables.....	xii
1. Introduction.....	1
1.1. Justification.....	1
1.2. Literature review.....	2
1.3. Objectives.....	8
1.3.1. Specific Objectives	8
1.3.2. Structure of the thesis.....	9
2. Theoretical background	10
2.1. Corrosion in metallic materials.....	10
2.1.1. Forms of corrosion	10
2.1.2. Dealloying.....	15
2.1.3. Selective Dissolution	17
2.2. Eutectic microstructure in al-cu system.....	18
3. Experimental procedure.....	20
3.1. Overview of the experimental procedure	20
3.2. Selection of chemical compositions.....	21
3.3. Melting and sample preparation	22
3.4. Free corrosion process.....	23
3.5. Characterization.....	23
4. Effects of solidification and annealing	24
4.1. Solidification issues	24
4.1.1. Diffusion during solidification.....	25
4.1.2. Formation of precipitates from solid solution.....	31

4.2. Solidification methods implemented	33
4.2.1. Quenching in cold water.....	33
4.2.2. Directional solidification	33
4.2.3. Quenching in a graphite mold	35
4.2.4. Solidification in copper molds	36
4.3. Annealing effect.....	40
5. Selective dissolution process	43
5.1. Free corrosion of directionally solidified samples	43
5.1.1. Samples without annealing.....	45
5.1.2. Annealed samples	48
5.2. Selective dissolution of samples solidified in copper molds	49
5.2.1. SEM study.....	50
5.2.2. Corrosion procedure	60
5.2.3. X-ray diffraction results	65
6. Conclusions and suggestions for future work.....	68
6.1. Conclusions.....	68
6.2. Suggestions for future work	69
References	71
Appendix.....	A1

LIST OF FIGURES

Figure 1: Classification of Nanoporous Materials [40]	7
Figure 2: Representation of galvanic corrosion [43]	12
Figure 3: Representation of crevice corrosion [43]	13
Figure 4: Representation of pitting corrosion [43]	14
Figure 5: Stress corrosion cracking representation [44]	15
Figure 6: Evolution of nanoporosity during dealloying [1]	16
Figure 7: Sketch of the interface shape of steady untilted eutectic growth [46]	18
Figure 8: Solidification of eutectics in hypoeutectic alloy, a) eutectic plane front, b) eutectic cells, and c) eutectic grains [45]	19
Figure 9: Overall procedure	20
Figure 10: Aluminum-rich side of the Al-Cu equilibrium phase diagram [48], [49]	22
Figure 11: Unidirectional solidification of Alloy C_0 with planar interface (above), and its corresponding composition profile (below). Assuming complete equilibrium [50].	26
Figure 12: Schematic phase diagram used to define equilibrium solidification [51].	27
Figure 13: Planar solidification front of alloy with nominal composition C_0 assuming no diffusion in solid, but complete mixing in the liquid [50]	28
Figure 14: Planar front solidification of alloy C_0 assuming no diffusion in solid and no stirring or convection in liquid. Above: front in the steady state region. Below: final transient [50].	29
Figure 15: Thermal profile during the solidification process [54].	31
Figure 16: Temperature ranges for heat treatment and relevant solvus lines for binary aluminum alloys in a schematic phase diagram [56]	32
Figure 17: Optical micrograph of EC sample directionally solidified (longitudinal section)	34
Figure 18: Optical micrograph of EC sample directionally solidified (cross-sectional view).	35
Figure 19: Optical micrograph of EC sample solidified in a graphite mold.	36
Figure 20: Mold used in solidification process, all units in mm.	37
Figure 21: SEM image of an EC sample solidified in a copper mold and corroded for 24 hours in 10 vol% NaOH aqueous solution.	38

Figure 22: SEM image of a HC-1 sample solidified in a copper mold and after corroded for 24 hours in 10 vol% NaOH aqueous solution. 39

Figure 23: SEM image of a HC-2 sample solidified in a copper mold and after corroded for 24 hours in 10 vol% NaOH aqueous solution. 39

Figure 24: Optical micrograph of Al-Cu eutectic alloy directionally solidified, longitudinal section view magnified more than in Figure 15..... 41

Figure 25: Optical micrograph of eutectic Al-Cu directionally solidified after annealing for 4 hours. 41

Figure 26: Optical micrograph of EC directionally solidified and annealed at 400°C for 24 hours. 42

Figure 27: SEM image of Al-Cu eutectic directionally solidified and corroded in 10 vol% NaOH aqueous solution for 4 hours..... 45

Figure 28: SEM image of Al-Cu eutectic colony in a directionally solidified specimen corroded in 10 vol% NaOH aqueous solution for 4 hours. 46

Figure 29: SEM image of the perimeter of Al-Cu eutectic colony in a directionally solidified specimen corroded in 10 vol% NaOH aqueous solution for 4 hours. 47

Figure 30: SEM image of a ligament detachment of in a eutectic Al-Cu specimen directionally solidified and corroded. 47

Figure 31: Optical micrograph of an EC sample corroded by 1 hour in NaOH (magnified 50X) 48

Figure 32: Optical micrograph of an Al-Cu eutectic sample corroded by 1 hour in NaOH with higher magnification than Figure 29. 49

Figure 33: Photographs of a HC-2 sample, a) before and b) after corrosion in 10 vol% NaOH for 24 hours..... 50

Figure 34: Surface of HC-2 sample after corrosion..... 51

Figure 35: Surface of EC sample after corrosion. 52

Figure 36: Example of steps for percent porosity estimation of one sample, a) original SEM photograph, b) elimination of areas that do not correspond to the observed cutting plane, c) conversion of the RGB image to binary image and inversion, where white areas correspond to pores, and d) boundaries of pores observed in the photograph..... 54

Figure 37: SEM image of the EC sample corroded to determine pore and ligament size. 55

Figure 38: SEM image of the HC-1 sample corroded to determine pore and ligament size. 55

Figure 39: SEM image of the HC-2 sample corroded to determine pore and ligament size. 56

Figure 40: Box plot of pore size for the three compositions studied..... 57

Figure 41: Box plot of ligament size for the three compositions studied. 58

Figure 42: SEM image of a HC-2 sample with formation of aluminum hydroxide during selective dissolution. 62

Figure 43: SEM image of a HC-2 sample with formation of aluminum hydroxide during selective dissolution (higher magnification than Figure 40).62

Figure 44: SEM image of EC sample with alumina formation due to incorrect treatment after corrosion.64

Figure 45: SEM image of aluminum oxide formation after selective dissolution in an EC sample.64

Figure 46: XRD diffraction pattern for EC sample uncorroded.66

Figure 47: XRD diffraction pattern for corroded EC sample.67

Figure 48: XRD diffraction pattern for EC sample corroded, without stirring during corrosion and aerated after that.67

LIST OF TABLES

Table 1: Summary of NPC from Al–Cu binary alloy.....	6
Table 2: Galvanic series [42]	11
Table 3: Observed reactions for samples directionally solidified in NaOH at different concentrations.	43
Table 4: Pore and ligament size measurements.....	57

1. INTRODUCTION

1.1. JUSTIFICATION

Precursor alloys for nanoporous metals (NPMs) are materials mainly constituted of two phases, in which one of them is removed by dealloying processing (selective dissolution). This process can be carried out by chemical or electrochemical corrosion [1].

These materials present important properties such as high adsorption capability, high selectivity, favorable adsorption kinetics, good stability, durability, and good mechanical properties, among others. In most cases, the pore size determines the performance of the material, for example the selectivity of an adsorbent depends of this factor [2]. Moreover, some properties are determined by the elements that make it up, as the NPMs are formed by the alloy of two or more metals such as gold, silver, copper, aluminum, etc.

There is a large number of applications of nanoporous metals. Some are employed in catalytic and optical applications [3], including nanoporous gold (NPG) obtained by electrochemical dealloying. The same set of NPG possesses important optical behavior because of the pores that can be modified by adjusting the pore size. Other applications can be found in biotechnology, sensing, energy-saving, and energy-generation technologies, among others [4].

Dealloying of metals has been studied as part of corrosion science, which considers at least nine forms: uniform, intergranular, galvanic, crevice formation, pitting, erosion, stress corrosion cracking, biological and selective leaching [5]. Furthermore, corrosion can present itself in more than one of those forms at the same time. In addition, for dealloying to occur two metals must be present, one nobler than the other. Consequently, the first dealloying studies focused on nanoporous gold, platinum, and silver [4], i.e. noble but expensive metals. For this reason, in the last years the research focus switched to less expensive metals such as aluminum, copper, zinc, nickel, magnesium. Unfortunately, dealloying of the latter is not as simple as in gold, silver, or platinum. Therefore, the ensuing methods of solidification and thermal treatments of the precursor alloys become more elaborate. Recently, researchers became interested in the dealloying of Al-Cu alloys [6]–[12]. However, there are many factors that affect this dissolution process, such as, alloy composition, solidification method, thermal treatment, type and concentration of chemical solution, corrosion temperature, and electrical potential applied. These factors are to be studied in this research to determine the optimal convergence of those factors to form nanopores in Al-Cu alloys.

1.2. LITERATURE REVIEW

Nanoporous metals can be obtained from selective dissolution, which is also called "*dealloying*". This process needs at least two phases in the alloy, in which one of those is removed, generating the pores. The remaining phase forms a ligament network, causing the sample to retain the initial volume, but its weight decreases naturally as the surface area increases.

Historically, selective dissolution was used primarily for chemical catalysis applications, e.g. in catalytic reduction of carbon oxides in the hydrocarbon production process, where heat transfer is very important. This led Philip White in 1944 to create a "*Raney catalyst surface*" [13], so called because of the Murray Raney patent in 1925 [14]. White was able to create this surface with alloys such as nickel–aluminum, cobalt–aluminum or nickel–cobalt–aluminum, where the aluminum phase could be replaced by silicon. The preferred composition range was between 35 - 65 weight percent of removable material, dissolved by an alkaline solution. White achieved a better heat transfer due to his new catalytic material, whereas Raney produced it for more general purposes, such as "*hydrogenation of animal, vegetable and fish oils, waxes, fats, hydrocarbon oils, and the like.*"

In 1963 Pickering and Swann [15] were, perhaps, the first ones to create nanoporous gold (NPG) in an attempt to study stress and corrosion cracking, using copper–gold. Through a transmission electron microscope (TEM) they recorded pores of up to 10 nm. The NPG study continued, this time on gold–silver alloy with 50:50 composition, using nitric acid as electrolyte for short times (60 s) and high temperatures (720 K) [16].

As the years passed, the selective dissolution studies expanded, for instance on iron–chromium–molybdenum alloys. In 1979 Leygraf et al [17] evaluated the surface enrichment of Cr and Mo polarized at constant potentials. In addition, constant current density applied to gold–silver alloys rendered smaller gold disperse particles formation [18].

As part of corrosion science, in the last years the dealloying process has achieved good results using gold, silver, platinum, and palladium, i.e. noble metals.

For instance, researchers used aluminum–gold–platinum alloy to create nanopores of gold–platinum (NPGPt) [19], employing hydrochloric acid (HCl) and sodium hydroxide (NaOH) with concentrations of 5 and 20 weight percent, respectively. This study also used corrosion at high temperatures (90°C) leading to ligament – pores sizes of 5.2 and 3.3 nm. Using the same electrolytes (HCl and NaOH) nanoporous silver (NPS) was obtained [20], and the removed element was aluminum with compositions between 15–60 atomic percent. However, the pores size, between 90–500 nm was much higher than in NPGPt. Moreover, platinum was used to create nanoporous platinum (NPt) [21], bearing ligament sizes of 7.2 nm.

To date, NPG has been the nanoporous metal with the best results with respect to ligament/pore size. Continuous research of this material encompassed different alloys, compositions, corrosion environment, applied potential, and, obviously, its applications. To form NPG the best way is starting from binary alloys, such as aluminum–gold [22], [23], tin–gold [24] and silver–gold [3], [25]–[28], which are etched in alkaline and acid solutions as HCl, NaOH and HNO₃. Others precursor binary alloys used to create nanoporous metals were nickel–manganese [29] and aluminum–magnesium [30]; in the first one nanoporous nickel (NPN), with pores up to 5–7 nm were obtained, by corrosion in (NH₄)₂SO₄ at different temperatures and long annealing times.

In the selective dissolution process, ternary alloys have also been used in innovative techniques encompassing various successive steps. For instance, NPG fabrication from aluminum–palladium–gold [31], started with dealloying to remove Al₂(Au,Pd) with NaOH, to form a Pd–Au nanoporous composite. The second dealloying stage with HNO₃ solution, rendered an Au–rich nanoporous structure. In another

multi-step process researchers developed nanoporous CuO ribbons [32] from an aluminum-gold-copper ternary alloy, producing nanoporous copper (NPC) first with some particles of gold by dealloying in NaOH. Subsequently, they performed surface oxidation and calcination.

Dealloying not only creates nanopores, but also other structures such as titania nanotubes [33] by using, titanium, aluminum, iron, molybdenum, and vanadium etched with NaOH anodized in H₃PO₄. The resulting nanotubes were in a range between 40– 80 nm.

Recently, nanoporous copper, mostly from binary alloys, has attracted much attention. For instance, copper-manganese [34] corroded at various solution concentrations of HCl resulted in pore sizes between 15–200 nm. Using alloys from the copper-zinc binary system can produce pores among 200–300 nm [35], 10–150 nm [25] and microporous copper (MPC) of 2 μm [36]. Physical vacuum dealloying generated large-size pores, without chemical dissolution.

The most used alloys to form NPC are aluminum-copper ones, usually corroded in an alkaline medium, e.g. NaOH, to remove the aluminum. Nevertheless, acid medium (HCl) and neutral solution (NaCl) have also proved effective. Both etchants have been employed at different concentrations with the precursor alloy composition from 25 to 50 atomic percentage of copper. These results are summarized in Table 1.

Upon dealloying, the precursor grain size affects the pore/ligament size in the resulting nanoporous metals. As a consequence, the solidification process of the precursor alloy becomes relevant to adjust the optimal grain size of that alloy. For this reason, rapid solidification is the most used method to achieve small grain sizes.

One remarkable tool is the single roller melt spinning apparatus that allows samples of a few tens of micrometers [8]–[11]. When the precursor ingots were prepared, they are annealed to form stable phases [6]. Other method used to control the grain size is mechanical alloying via ball-milling to form the Al_2Cu intermetallic phase to produce NPC [12].

Table 1: Summary of NPC from Al–Cu binary alloy

Precursor alloy (at %)	Solution	Pore size (nm)	Ligament size (nm)	Reference
$\text{Al}_{75}\text{Cu}_{25}$ & $\text{Al}_{67}\text{Cu}_{33}$	NaCl	50 – 200	~	[6]
$\text{Al}_{75}\text{Cu}_{25}$	NaOH	10 – 50	10 – 50	[7]
$\text{Al}_{85}\text{Cu}_{15}$	HCl	~	60 – 120	[8]
$\text{Al}_{100-x}\text{Cu}_x$, $x = 33, 35, 40, 50$	NaOH	20 – 200	20 – 200	[9]
$\text{Al}_{100-x}\text{Cu}_x$, $x = 33, 35, 40, 50$	HCl & NaOH	~	100 – 500	[10]
$\text{Al}_{65}\text{Cu}_{35}$	NaOH	~	25 – 350	[11]
	NaOH	25 ± 20	30 ± 20	[12]

In other works on NPC the authors used ternary alloys such as aluminum–copper–magnesium [37] and aluminum–copper–hafnium [38]. The first compared the effect of nickel as aggregate at three atomic percent; this method permitted to reduce the pore/ligament size from 20– 30 to 10–20 nm. Moreover, the alloy containing hafnium attained pore sizes between 15–140 nm.

In all research reported thus far, when aluminum was present it was the sacrificial element. One report described nanoporous aluminum (NPAI) formation [39] with pores with less than 100 nm in diameter using HNO_3 under an applied electrical field.

Currently, nanoporous metals (NPMs) continue to be widely studied due to their previously mentioned properties and applications, along with other nanoporous materials, as shown in Figure 1. In summary, great strides have been made in

Materials Science, where the NPMs are part of a relatively new branch with few decades of development. Accordingly, this literature review demonstrates that nanoporous metals have not been previously prepared from intermetallic phases in precursor aluminum–copper alloys. A new material could be produced starting from binary Al–Cu alloys having an intermetallic Al_2Cu phase (θ) and primary αAl phase in appropriately similar volume fractions. Obtaining such a porous material may lead to an innovative catalyst with properties never seen before.

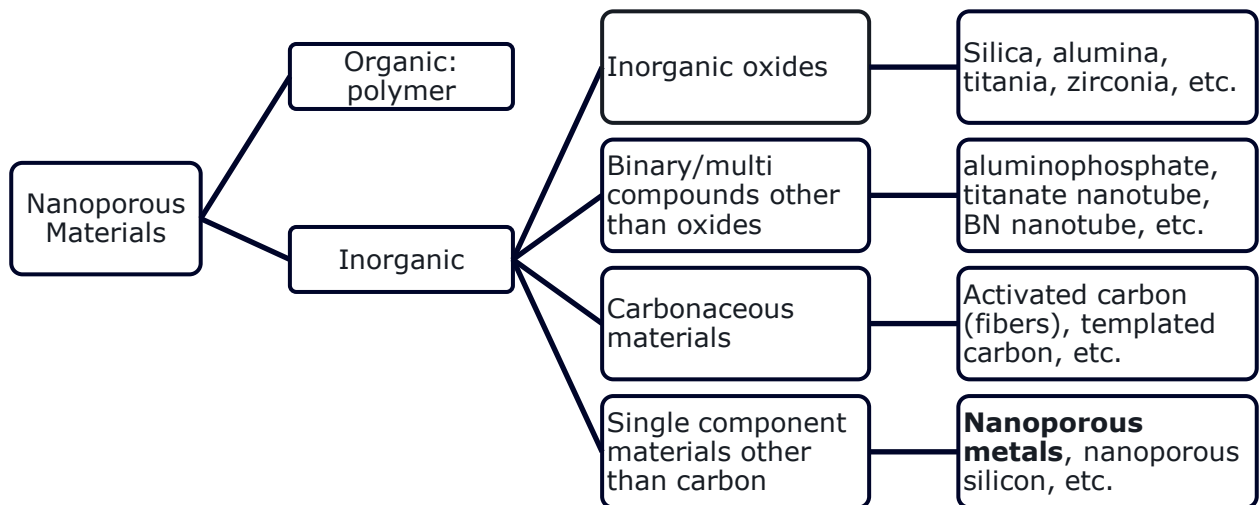


Figure 1: Classification of Nanoporous Materials [40]

1.3. OBJECTIVES

The present research seeks to formulate a porous metal through selective dissolution of aluminum-copper alloys bearing different compositions as precursors. The solidification process was also studied to analyze the effect of the precursor microstructure in the dissolution process under free corrosion. This helped determine the optimal values of the solidification and corrosion factors that affect the formation of pores and ligaments of homogeneous size in the porous metal. In closing, the project sought to establish a methodology to attain nanoporous metals with relatively low cost of fabrication.

1.3.1. Specific Objectives

- Determine the optimal composition of a precursor binary Al-Cu alloy that renders high porosity in the porous metal.
- Establish the effect of the solution concentration on the final pore and ligament sizes in the nanoporous material.
- Design the solidification method that renders an alloy with a fine microstructure, adequate for the selective dissolution process.
- Characterize the samples by x-ray diffraction (XRD) to determine the effectiveness of the dissolution process.
- Characterize the dealloyed samples by optical microscopy and scanning electron microscopy (SEM) to determine the average ligament and pore size.

1.3.2. Structure of the thesis

Chapter 2 provides the theoretical background concerning corrosion in metals and a short overview about eutectic structures present in the Al-Cu system. Chapter 3 details the experimental procedure implemented to prepare nanoporous metals from Al-Cu alloys. Chapter 4 describes the effect of solidification methods and the subsequent annealing process over the alloy microstructure. 5 delineates the corrosion process as it was used in the selective dissolution of one phase from Al-Cu alloys. This chapter also presents preliminary work on to selective dissolution from directionally solidified samples with eutectic composition. The selective dissolution is explained for three different compositions solidified in copper molds; also the obtained pore and ligament size in this process is analyzed. Finally, the conclusions and suggestions for future work are included in Chapter 6.

2.THEORETICAL BACKGROUND

2.1. CORROSION IN METALLIC MATERIALS

2.1.1. Forms of corrosion

As aforementioned, metallic materials may be affected by eight forms of corrosion [5], [41]:

Uniform corrosion

This may be the simplest form of corrosion observed in metals. In this mechanism, it is enough for the material to be exposed to a corrosive environment, which can simply be air. This makes the oxygen present react with the metal and corrodes uniformly its surface. In metals like aluminum, the surface corrosion leads to a passivating oxide that protects the metal underneath from further corrosion by isolating it from the oxidizing medium. However, in metals such as steel, the metal oxide layer becomes porous causing the rest of the material to be exposed to the corrosive environment and in this way the process continues until all the metal is oxidized.

Intergranular corrosion

This localized corrosion occurs on the grain boundaries and quickly spreads through the material, causing fractures and metal failure.

Galvanic corrosion

It occurs when two metals have electrical contact under the same corrosive environment (electrolyte, e.g. air or sea water). The different electrochemical nature of the metals leads to a potential difference between those two, causing the less noble element to be corroded (losing electrons). This type of corrosion is quite common, since in many industries metals of different nature are used in a single assembly or part. For instance, aluminum structures can be in contact with galvanized steel reinforcements. In this case, the steel is less noble than aluminum, causing the light metal to lose electrons over time, which becomes detrimental to the structural mechanical properties. Table 2 shows the descending order of the nobility of some metals, according to the galvanic series.

Table 2: Galvanic series [42]

Magnesium (less noble)	Zinc (2 nd less noble)	Beryllium
Cadmium	Uranium	Aluminum
Indium	Tin	Lead
Iron (cast)	Copper	Chromium
Tantalum	Tungsten	Niobium
Yellow Brass	Brass (plated)	Bronze 220
Red Brass	Molybdenum	Bronze

Silver	Gold	Graphite (most noble)
--------	------	-----------------------

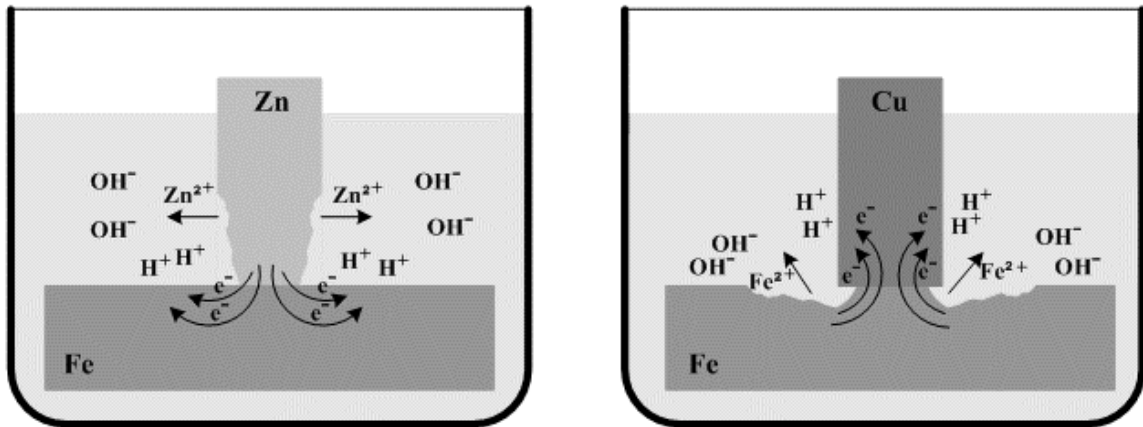


Figure 2: Representation of galvanic corrosion [43]

Crevice corrosion

As in intergranular form of corrosion, this is a localized corrosion, caused by narrow gaps or openings formed between metals and another type of non-metallic material. Corrosion occurs due to differences in oxygen concentration as the metal oxide is deposited adjacent to the non-metallic material on the metal surface (Figure 3). This type of corrosion is considered much more harmful than uniform corrosion, as it occurs at faster speeds (between 10-100 times faster).

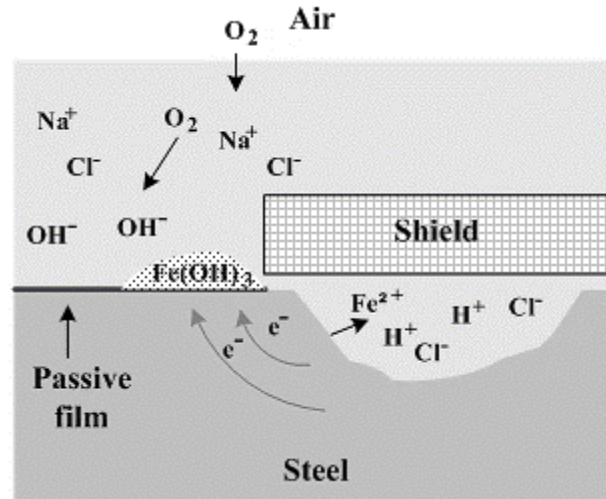


Figure 3: Representation of crevice corrosion [43]

Pitting

This highly localized corrosion occurs when a metal becomes exposed to a corrosive medium (e.g., steel in contact with or immersed into sea water) and a defect appears in the protective layer or surface. This defect can be a small hole, through which the corrosion leads to a tiny but deep hole that increases with time. This causes a significant loss in the thickness of the metal, compromising its mechanical properties. Since it is a highly localized type of corrosion, it is difficult to find it by ocular inspection.

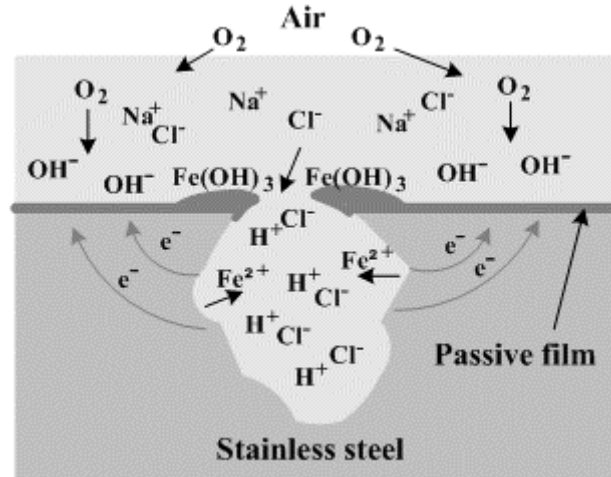


Figure 4: Representation of pitting corrosion [43]

Erosion corrosion

It occurs when a corrosive liquid flows through a metal pipe, in which the speed of the fluid displacement plays an important role, since the relationship between this factor and corrosion by erosion is directly proportional. The laminar flow becomes less destructive, as the turbulent one increases the contact of the liquid with the metal surface.

Stress corrosion cracking

When a metal is exposed to a corrosive environment as a force is applied to it, stress corrosion cracking may occur. The conditions for metal failure also depend on the pH of the corrosive environment, the metal susceptibility, and the mechanical stress level. During the corrosion process, fine cracks penetrate from the metal surface to the stress points and can spread via intergranular regions.

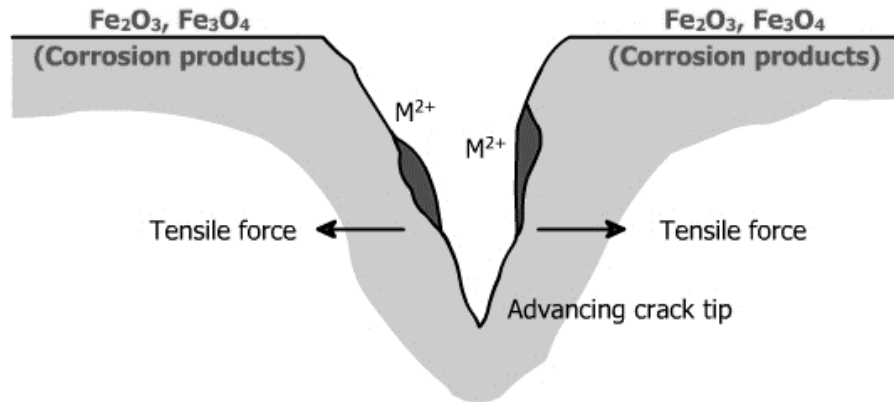


Figure 5: Stress corrosion cracking representation [44]

Selective leaching

This process occurs intentionally (unnaturally) when a metal or phase in a metal alloy is removed selectively, as the other metal or the other phase remains untouched. This creates a network of ligaments of the remaining phase. In the review of the literature and the development of this thesis this is the type of corrosion sought.

2.1.2. Dealloying

This is a form of selective leaching where an element present in a metal alloy is removed regardless of whether it is in a primary or intermetallic phase. Erlebacher [1] mentions four characteristics that alloys must have to achieve dealloying. If these four conditions do not occur, corrosion may be removing not only the less noble metal:

- a. There must be a significant difference in potential between the elements that are to be dissociated.

- b. The composition must be rich in the element that remains, that is, the nobler element.
- c. The diffusion of the element in the electrolyte must be fast enough.
- d. The alloy should be sufficiently homogeneous and ideally stress-free.

The porosity evolution is illustrated in Figure 6. Initially the alloy is exposed to the corrosive medium (electrolyte) and the less noble element begins to react chemically with such electrolyte, causing it to dissolve in it, forming a pit. As the atoms of the less noble element are removed, free atoms of the nobler element (adatoms) remain, which by diffusion are agglomerated in certain regions with other atoms of the same element. When the pit grows, the adatoms are accommodated in new regions, as larger distances reduce the diffusion process. New atom clusters form and create a network of interconnected ligaments as the detachment of more atoms of the less noble element evolves.

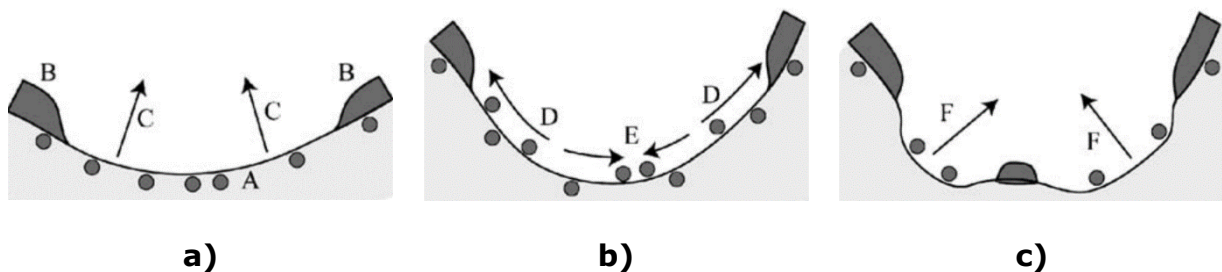


Figure 6: Evolution of nanoporosity during dealloying [1]

Thanks to diffusion during the porosity evolution in the dealloying process, some alloys can change crystalline structure, e.g. nanoporous copper, in which initially two phases coexist, α -Al and θ -Al₂Cu. In this case, the sacrificial element is Al, since it is the less noble of those two. The other phase, i.e. Al₂Cu, has a tetragonal structure

and by removing the aluminum from both the primary and intermetallic phases, copper adatoms form the FCC structure characteristic of copper.

2.1.3. Selective Dissolution

Dealloying is a type of selective leaching. In this process the removed phase is not necessarily made up of a single element. Similarly, the remaining phase can also be an intermetallic (not of a pure element or a solid solution of a given element) as in the dealloying case.

Generally, selective dissolution is achieved through free or spontaneous corrosion. Thus, an applied electrical potential may not be necessary to favor the process, as one of the phases and the electrolyte react chemically. Hence, this phase dissolves into the electrolyte as the other phase remains. As in the dealloying process, the four aforementioned aspects are also needed in an effective selective corrosion process. Yet, in selective dissolution, the fourth characteristic is even more important because electrical potential is not applied, and the reduction process is not favored. In other words, diffusion does not occur and more mass can pass into the electrolyte, causing that at the end of the corrosion process, the sample can be destroyed.

As no diffusion occurs in this process, in the end the metal microstructure defines the resulting material porosity. Hence, it is preferable that only two phases be present in the alloy; otherwise, more phases would involve more complex chemical reactions in which the process may not be selective.

2.2. EUTECTIC MICROSTRUCTURE IN AL-CU SYSTEM

In this research, samples with compositions close to the eutectic point of Al-Cu alloy were corroded. Therefore it was important to characterize the eutectic structures that can appear after the solidification of the metal, since such structure determines the ligaments morphology and the final porosity of the material.

In the Al-rich side of the Al-Cu binary system, the type of eutectic structure is laminar, constituted by Al and θ phases (Figure 7). In this regular eutectic, the volume fractions of both eutectic phases are similar, with the lamella of both phases bearing similar thicknesses. This means that the interlaminar distance tends to be uniform. However, phase growth will not always occur as a eutectic plane front. Further, the solidification microstructure can be eutectic cells or eutectic grains [45].

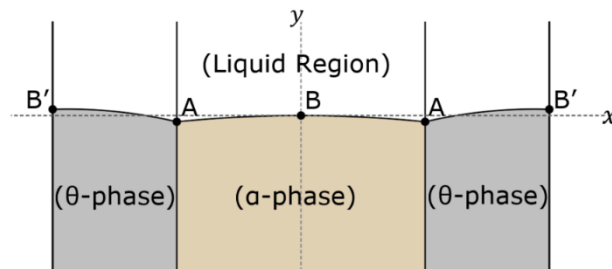


Figure 7: Sketch of the interface shape of steady untilted eutectic growth [46]

The difference between the three types of eutectic structures in Figure 8 depends on the impurities present in the material [45] and/or on the critical rate of solidification [47]. The proeutectic primary dendrites shown in the figure correspond to α Al if the composition is hypoeutectic or θ if it is hypereutectic.

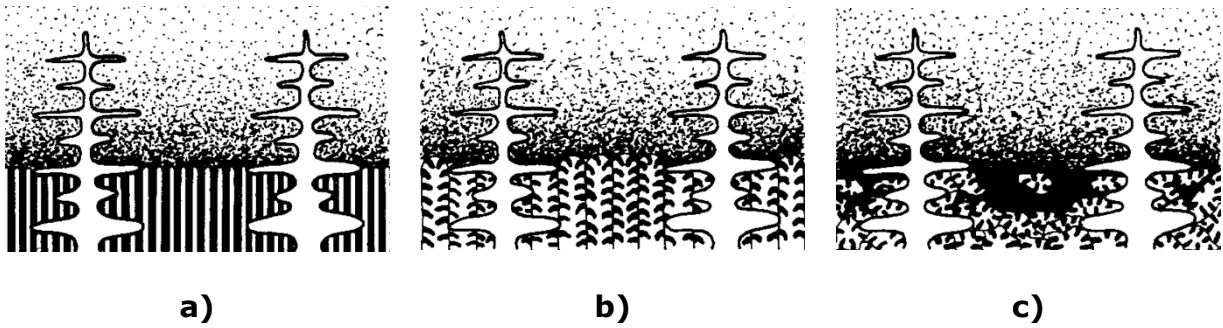


Figure 8: Solidification of eutectics in hypoeutectic alloy, a) eutectic plane front, b) eutectic cells, and c) eutectic grains [45]

3. EXPERIMENTAL PROCEDURE

3.1. OVERVIEW OF THE EXPERIMENTAL PROCEDURE

Figure 9 provides the overarching procedure used in the present research.

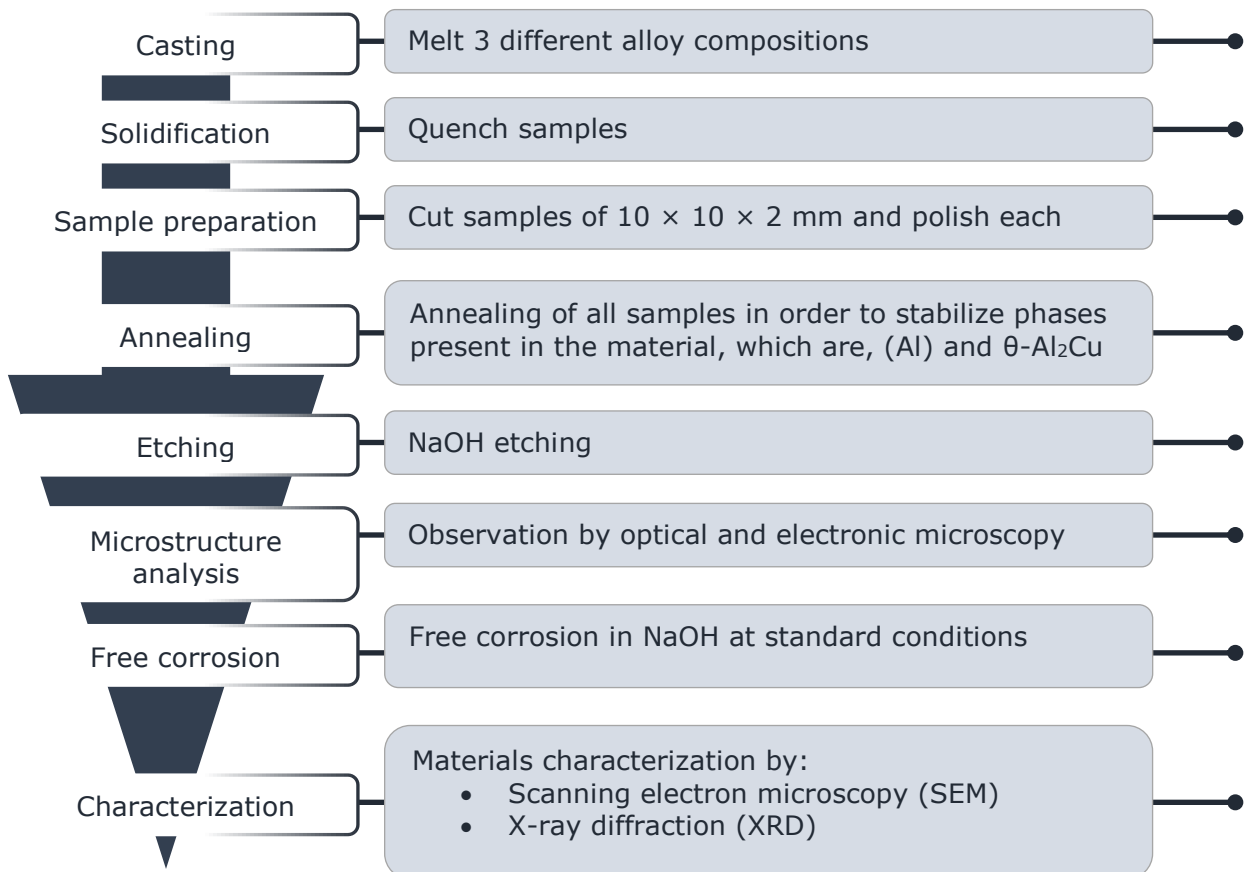


Figure 9: Overall procedure

This was the final methodology, which required several steps. Casting is described in this section; solidification and annealing are detailed in the next section.

Etching was performed to reveal the sample microstructure observed using optical microscopy. Furthermore, free corrosion process was performed for extended periods, namely 24 hours. Additionally, materials characterization is described below.

3.2. SELECTION OF CHEMICAL COMPOSITIONS

As already mentioned, solidification affects the samples corrosion as, under free corrosion, the sample porosity will depend on the microstructure of the alloy. Further, assuming total dissolution of one alloy phase, the minimum theoretical volume of the remaining phase should be at least a fifty volume percent. We believe that this would be the limiting composition to avoid sample crumbling. In an aluminum–copper alloy, this can be achieved using the 33.2 wt% Cu eutectic composition.

In the Al-Cu partial phase diagram in Figure 10, the three compositions studied are shown. These were selected based on their θ phase volume percent, which is 50, 55, and 60 volume percent in the compositions Al-17.52 at% Cu, Al-19.17 at% Cu, and Al-20.80 at% Cu respectively. Hereinafter, we call these compositions: EC, HC-1 and HC-2. The main goal is to increase the sample area as much as possible. Therefore, in theory, the eutectic composition should be the most porous sample. However, this composition is the limit for the formation of ligaments, which must be interconnected to avoid sample destruction. For this reason, other two compositions with a higher volumetric percent of the remaining phase were studied.

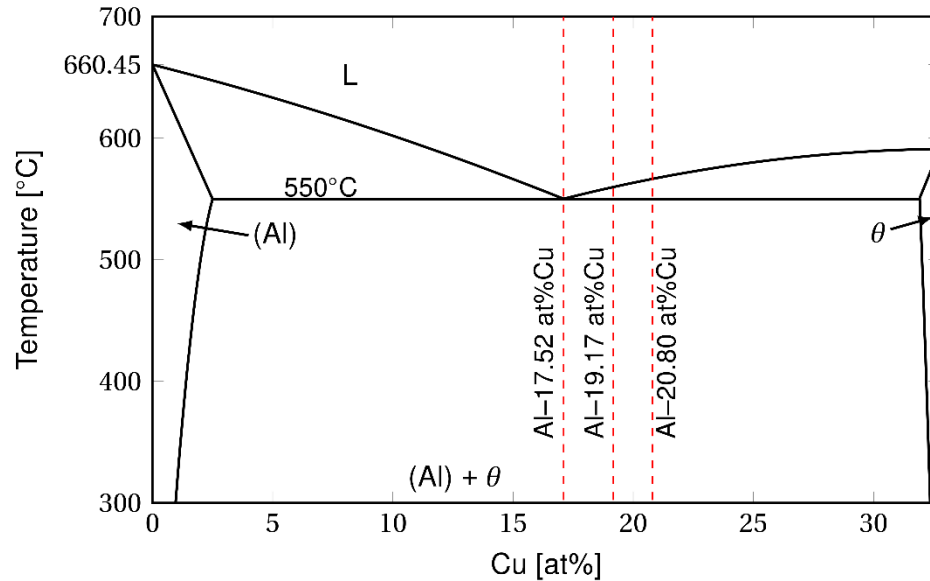


Figure 10: Aluminum-rich side of the Al-Cu equilibrium phase diagram [48], [49]

3.3. MELTING AND SAMPLE PREPARATION

The three aforementioned compositions were melted in a graphite crucible at about 800°C for about 30 minutes using an Al-33 wt% Cu master alloy obtained from Milward Alloys, Inc. To adjust the alloy compositions, we added pure copper metal chunks.

In order to obtain a fine microstructure, three solidification methods were tested: directional solidification, quenching in graphite mold, and solidification in copper molds. After all those treatments and to stabilize the microstructure, the samples were annealed at 400°C for 24 hours. The portions that solidified in direct contact with the molds were discarded, since they can present a very different microstructure (chilled regions), causing non-uniformity in pore and ligament sizes within each sample. Subsequently, the annealed samples were cut as 10 × 10 × 2 mm specimens to be polished with a 0.1 μm finishing.

3.4. FREE CORROSION PROCESS

In this process, each sample was placed in a 100 ml NaOH solution with different concentrations, i.e. from 1 to 25 vol%, at room temperature. The samples were kept in the corrosive medium for at most 24 hours or until no bubble formation was observed. This would indicate that the oxidation process had stopped. Thereupon, the samples were removed, placed in distilled water in a sonicator for 20 minutes, and immediately immersed into ethanol for 5 minutes in the same sonicator to stop the corrosive process. Finally, the samples were placed in an oven at 100°C for 8 hours to remove any moisture present.

3.5. CHARACTERIZATION

To characterize the new material, we used x-ray diffraction, optical microscopy, and scanning electron microscopy. XRD was used to determine and corroborate the phases present in the material before and after corrosion. This was done in a Siemens D500 x-ray diffractometer with a copper target and operated with sampling 2θ angles between 10° and 80° .

Additionally, the samples were observed in a metallographic optical microscope and in an SEM to determine the porosity of the material. This allowed measuring the pore size and ligament. The SEM used was a JEOL JSM-7610F FEG-SEM.

4. EFFECTS OF SOLIDIFICATION AND ANNEALING

In selective dissolution, the attained porosity depends directly on the microstructure of the parent (precursor) alloy. In addition, the best way to simplify the subsequent chemical reactions is by having only two phases present in the alloy. Thus, for the studied compositions, a primary aluminum phase and the intermetallic Al_2Cu coexist. These two phases are stable according to the Al-Cu equilibrium phase diagrams. However, the type of solidification and the subsequent thermal treatment determine the final volume fractions of these phases and their chemical stability.

4.1. SOLIDIFICATION ISSUES

During solidification, several issues can arise as a consequence of a high temperature gradient and significant cooling rates. Such circumstance makes the present phases in the material lack an ideal formation as the equilibria phase diagram indicates. Formation of precipitates from solid solution is one of these issues. In principle, one can attribute these happenings to the compromised diffusion during solidification and cooling.

4.1.1. Diffusion during solidification

In the Al-Cu system, eutectic Al and Al₂Cu lamellas grow in a cooperative manner. This growth is subject to the rapid diffusion in the liquid adjacent to the solidification front. This governs then the lamellar spacing. Generally, a small interlaminar spacing leads results from rapid growth [50]. Further, several solidification instances can be considered depending on the cooling rate.

Equilibrium solidification

In this case we can assume an infinitely slow solidification cooling rate. Hence, the compositions of phases follow strictly the phase equilibria diagram. Because there is an extended solidification, the diffusion is favored and the alloy composition satisfies the lever rule. Figure 11 shows this case, where C_L is the liquid composition; C_S , the solid phase composition; and C_0 , the alloy nominal composition. In this figure, x represents the position of the solidification front, assuming unidirectional growth. Complete equilibrium (infinitely slow solidification) of the eutectic alloy renders wide lamellar formation. For this reason, this solidification method was not selected for this research.

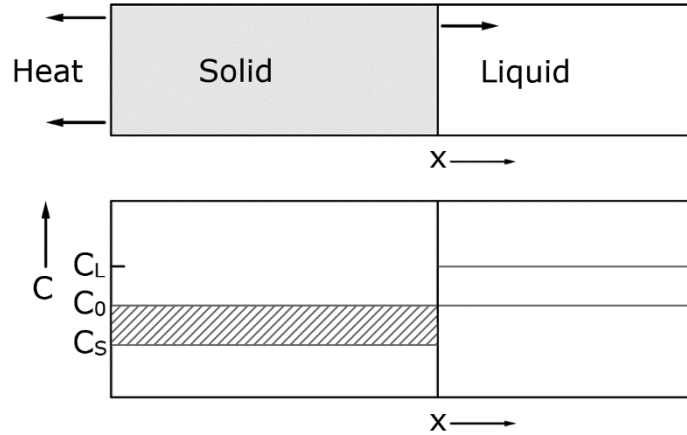


Figure 11: Unidirectional solidification of Alloy C_0 with planar interface (above), and its corresponding composition profile (below). Assuming complete equilibrium [50].

In this case, one can assume conservation of solute atoms and define an expression for the solid concentration in any region of T^* (Figure 12).

$$C_S f_S + C_L f_L = C_0 \quad \text{with} \quad f_S + f_L = 1 \quad (1)$$

where f_S and f_L are the mass fraction of solid and liquid; thus, the solid composition is:

$$C_S = \frac{k C_0}{1 - (1 - k) f_S} \quad (2)$$

Equation (2) assumes $\rho_S = \rho_L$, but when these densities are not equal,

$$C_S = \frac{1 - (1 - \rho_S/\rho_L) f_S}{1 - (1 - k \rho_S/\rho_L) f_S} k C_0 \quad (3)$$

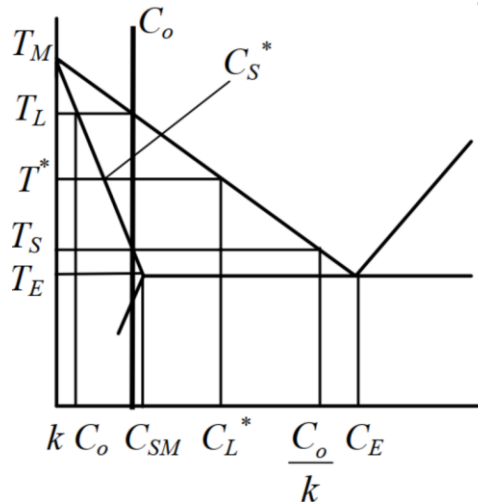


Figure 12: Schematic phase diagram used to define equilibrium solidification [51].

No diffusion in the solid and perfect mixing in liquid

On the other hand, solidification with perfect mixing (infinite diffusion) in the liquid would allow a finer microstructure. However, in solid solution the concentration of solute changes through the advancing solidification front. Figure 13 depicts this case, where k represents the partition coefficient, defined as $k = C_S/C_L$. To promote homogeneity in the liquid phase, this type of solidification requires a vigorous stirring, which is quite complicated to carry out when solidification takes place.

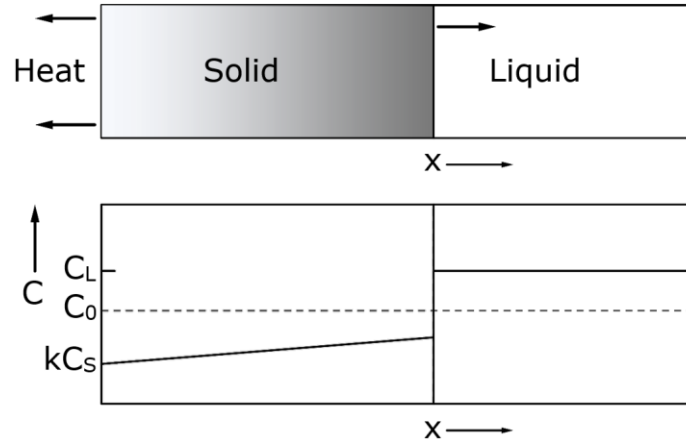


Figure 13: Planar solidification front of alloy with nominal composition C_0 assuming no diffusion in solid, but complete mixing in the liquid [50].

Assuming this case, the solute is rejected at solidification front, raising the solute concentration in the liquid phase. Then, the mass fraction is changing as the solidification front advances:

$$(C_L - C_S) df_S = (1 - f_S) df_S \quad (4)$$

After mathematical manipulation, the concentration of solid phase becomes:

$$C_S = k C_0 (1 - f_S)^{k-1} \quad (5)$$

No diffusion in solid and diffusional mixing in liquid

Without stirring or convection in liquid phase, the solute rejected in the interface raises its concentration ahead of the solidification front, as depicted in Figure 14. This case somewhat resembles real solidification conditions of the present study. The solidifying phase starts with a solute concentration of kC_0 and increases until reaching the composition C_0 . At that point a steady state begins, i.e. the composition in the solid phase remains constant. When the solidification front is forwarding in the steady state zone, the composition ahead of the solidification front is steady at C_0/k . When

the solidification front reaches the limit, the composition increases up to the eutectic alloy composition, C_E . Hence, the solid phase formation does not have a uniform diffusion of solute along the local solidification direction. This brings forth an issue related to the corrosion susceptibility, as the chemical reactions will be different under distinct solute concentrations. Furthermore, this alloy would not be sufficiently homogeneous to render a stress-free specimen. This latter problem could cause the sample to have a detachment of ligaments, in spite of the selective corrosion process.

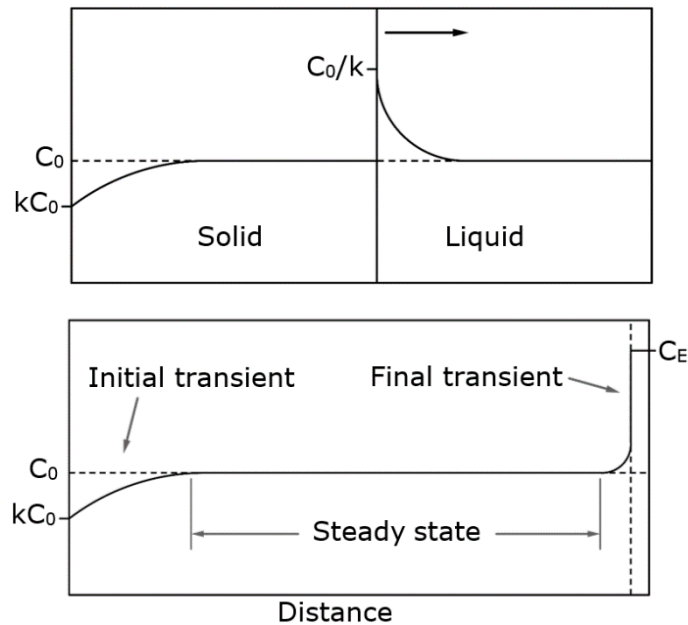


Figure 14: Planar front solidification of alloy C_0 assuming no diffusion in solid and no stirring or convection in liquid. Above: front in the steady state region. Below: final transient [50].

Assuming constant density and diffusivity and unidirectional solidification, the equation that describes the diffusion process is:

$$\frac{\partial^2 C}{\partial x^2} - \frac{V}{D} \frac{\partial C}{\partial x} = \frac{1}{D} \frac{\partial C}{\partial t} \quad (6)$$

The solution for the equation (6) is:

$$C_S = C_0 \left[1 - (1 - k) \exp\left(-k \frac{V}{D} x\right) \right] \quad (7)$$

Where V and D represents the velocity and diffusion coefficient respectively [51].

The mathematical model for temperature along the solidification direction (Figure 15) can be described taking in account other assumptions [52]–[54]:

1. The conductive flow is unidimensional.
2. The material properties are invariant within the same phase.
3. In the liquid only, conductive flow is considered.

With these conditions, the temperature in solid is:

$$T_1 = T_0 + \frac{T_S - T_0}{\text{erf}(\Phi_1)} \text{erf}\left(\frac{x + 2 \Phi_2 \sqrt{a_2 t_0}}{2 \sqrt{a_1} (t + t_0)}\right) \quad (8)$$

In the mushy zone:

$$T_2 = T_L - \frac{T_L - T_S}{\text{erf}(\Phi_2) - \text{erf}(n \Phi_1)} \left[\text{erf}(\Phi_2) - \text{erf}\left(\frac{x + 2 \Phi_2 \sqrt{a_2 t_0}}{2 \sqrt{a_2} (t + t_0)}\right) \right] \quad (9)$$

The temperature in liquid becomes:

$$T_3 = T_P - \frac{T_P - T_L}{1 - \text{erf}(m \Phi_2)} \left[1 - \text{erf}\left(\frac{x + 2 \Phi_2 \sqrt{a_2 t_0}}{2 \sqrt{a_3} (t - t_0)}\right) \right] \quad (10)$$

where,

- a Thermal diffusivity (m^2/s)
- m Constant of metal = $(a_2/a_3)^{1/2}$ (dimensionless)
- n Constant of metal = $(a_1/a_2)^{1/2}$ (dimensionless)
- t Time
- T_0 Temperature of mold (K)
- Φ Solidification constant (dimensionless)

Subscripts:

1. Solid metal

2. Mushy zone
3. Liquid metal

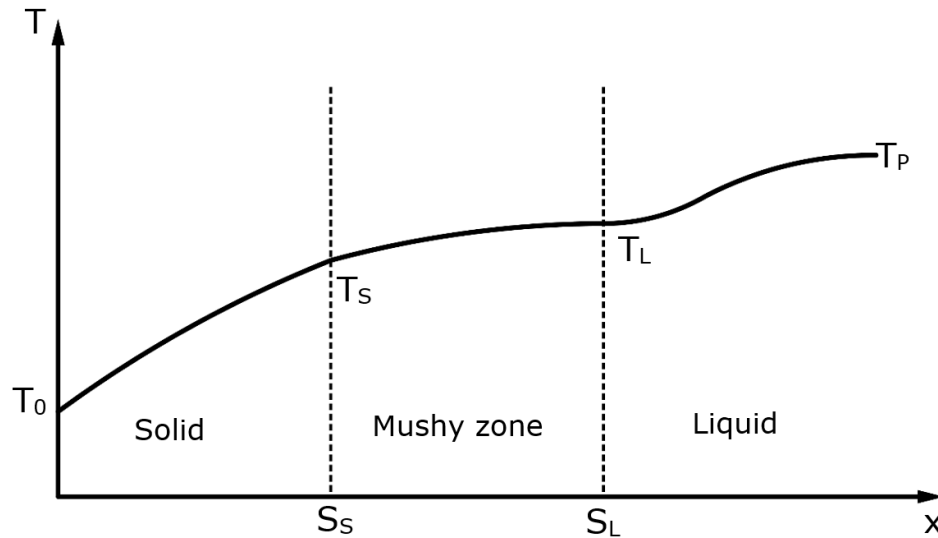


Figure 15: Thermal profile during the solidification process [54].

4.1.2. Formation of precipitates from solid solution

When we use liquid quenching or rapid solidification, the resulting microstructure may not be the two stable phases already mentioned, as some metastable phase or precipitates could form. Those metastable precipitates could, for instance, be Guinier–Preston (GP) zones or other binary structures. As depicted in Figure 16, depending on the heat-treating temperature, different material properties can be achieved. For instance, after quenching some Al-Cu alloys can be hardened by aging at relatively low temperatures, normally lower than 200°C.

The GP solvus indicates that this metastable precipitate can form depending on the temperature after solidification by quenching or also rapid solidification. This causes the alloy to retain a different composition than those indicated by the equilibrium phase diagram. Therefore, through ageing and depending on its

temperature, there is a metastable precipitation sequence: GP zones, θ'' , and θ' [47]–[49]. Only upon overageing the stable phase θ (or Al_2Cu) forms. However, to accelerate the process of achieving the stable phase θ , the temperature can be raised to favor the diffusion process. Normally, such annealing treatment is applied to aluminum alloys between 260 to 440°C and is used to improve the material ductility. The treatment not only improves this property, but it could also help stabilize the microstructure of the alloy by forming the stable phases (according to the equilibrium phase diagram), lowering its corrosion susceptibility [55]. However, one must notice that the annealing temperature should not be too high, i.e. close to the eutectic temperature, as Al-Cu alloys tend to form “coring” for lack of diffusion of the solute in the solid [50]. The homogenization via annealing could also result in excessive grain growth that would defeat the purpose of this treatment for our intended application.

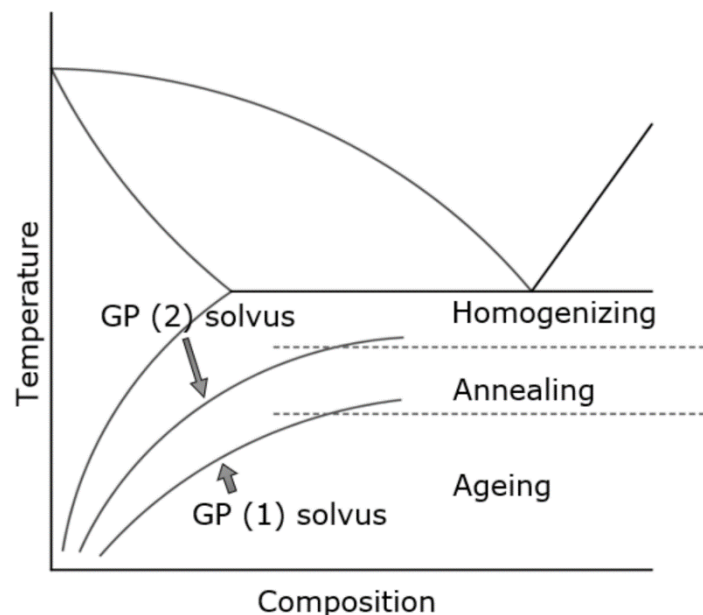


Figure 16: Temperature ranges for heat treatment and relevant solvus lines for binary aluminum alloys in a schematic phase diagram [56]

4.2. SOLIDIFICATION METHODS IMPLEMENTED

There are several solidification processes available for these alloys. The ones selected were those that render finer microstructures in order to produce finer pores after selective dissolution of the precursor alloy.

4.2.1. Quenching in cold water

Upon liquid quenching the melt was poured directly into water or other liquid so that a high solidification rate was attained by fast heat extraction. Nevertheless, this process is not efficient to grant a large enough thermal gradient, as evidenced by prior results on the dendritic growth of an Al-Zn alloy [39]. In that research, quenching in liquid nitrogen caused larger interdendritic spacing than in cold water quenching. This was likely due to the formation to a sheath of nitrogen gas enclosing the hot specimen, which prevented faster heat transfer. Even so, in this research we tested this type of solidification and found it inconvenient since the solidified sample ended up with excessive porosity (mostly due to fast vaporization of the liquid). Such porous precursor specimen was inadequate for the corrosion process, as the area exposed to the electrolyte was extreme, leading to pitting corrosion (not selective) as well as to sample brittleness. Therefore, liquid quenching was discarded for this study.

4.2.2. Directional solidification

Figure 17 and Figure 18 are micrographs of eutectic Al-Cu samples directionally solidified, in which the solidification direction of the main branches is shown. Via the

directional solidification method, the grain growth direction can be controlled, which is useful in adjusting the pore structure. In the longitudinal view (Figure 17) there are different thicknesses of eutectic lamellar structure, with finer lamellae at the center of the colonies in Figure 18. In these photographs, the light areas correspond to the α Al-phase, and the dark ones to the Al_2Cu -intermetallic phase. Furthermore, at the center of the colonies, formation of thin eutectic lamellas can be seen. Whereas the border of the colonies for both phases, a structure with thicker phase areas than the center is presented. Still, the pore and ligament sizes presented have too large a variability, making it difficult to analyze the actual solidification effect.

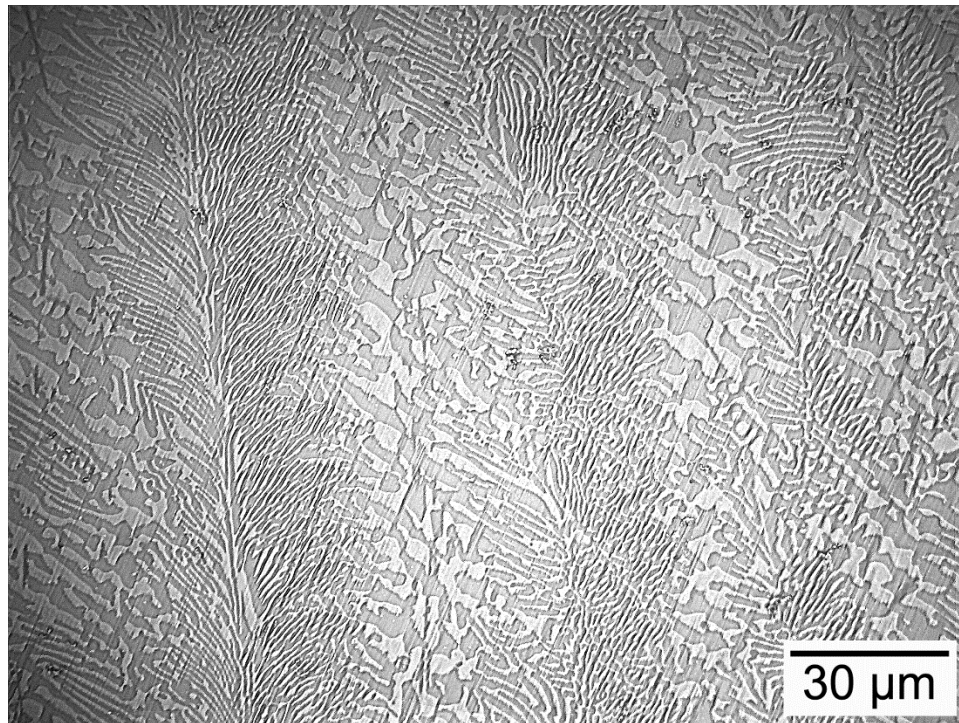


Figure 17: Optical micrograph of EC sample directionally solidified (longitudinal section).

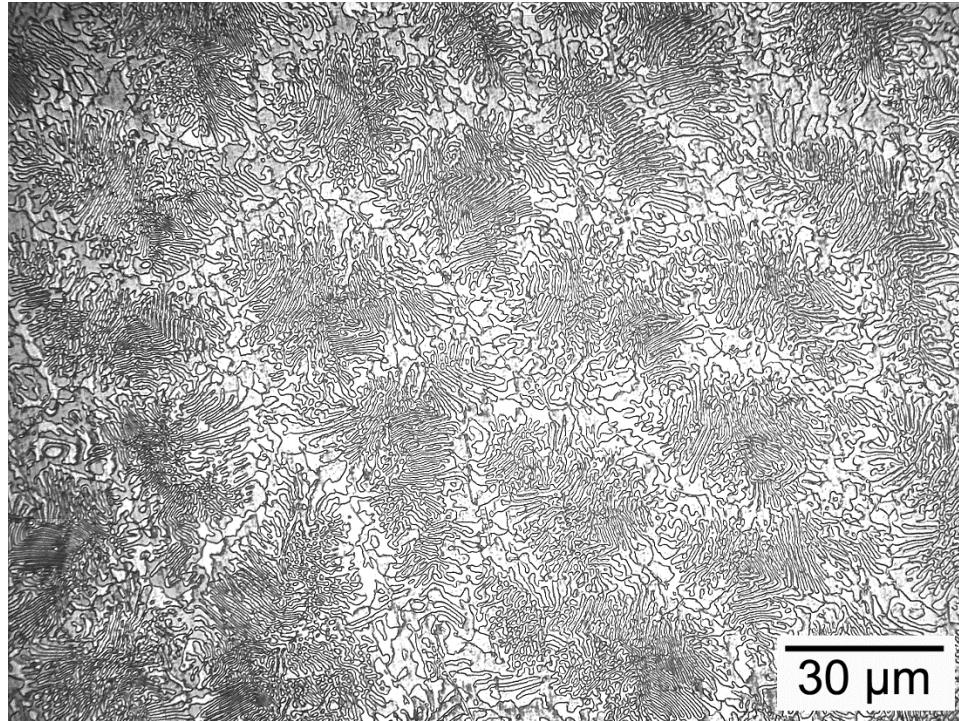


Figure 18: Optical micrograph of EC sample directionally solidified (cross-sectional view).

4.2.3. Quenching in a graphite mold

Hereafter, rapid solidification was carried out by only regular quenching, i.e. without pouring the melt into a liquid. This was done by pouring the crucible content into a mold at the same temperature ($\sim 800^{\circ}\text{C}$) and immersing it immediately into cold water ($\sim 5^{\circ}\text{C}$). This procedure eliminated the porosity problem in the precursor alloy. The microstructure, however, continued not to be fine enough (Figure 19). Using this method, directional and non-directional solidification processes were carried out.

For this process, we heated a graphite mold at the same temperature as the molten alloy, i.e. 800°C . This was a cylindrical graphite mold with a 25 mm diameter to hold the molten sample as the entire array was immersed in cold water ($\sim 5^{\circ}\text{C}$).

This setup attained a fast cooling rate without exposing the melt directly to a cold liquid. The mold shape and the direction and magnitude of the heat transfer generated a non-uniform microstructure: finer near the mold walls and thicker in the ingot center. As a result, we ruled out this solidification method since it could not render a homogenous pore size due to the heterogeneous microstructure throughout the sample. Additionally, the lamellar spacing achieved was too large for nanopores.

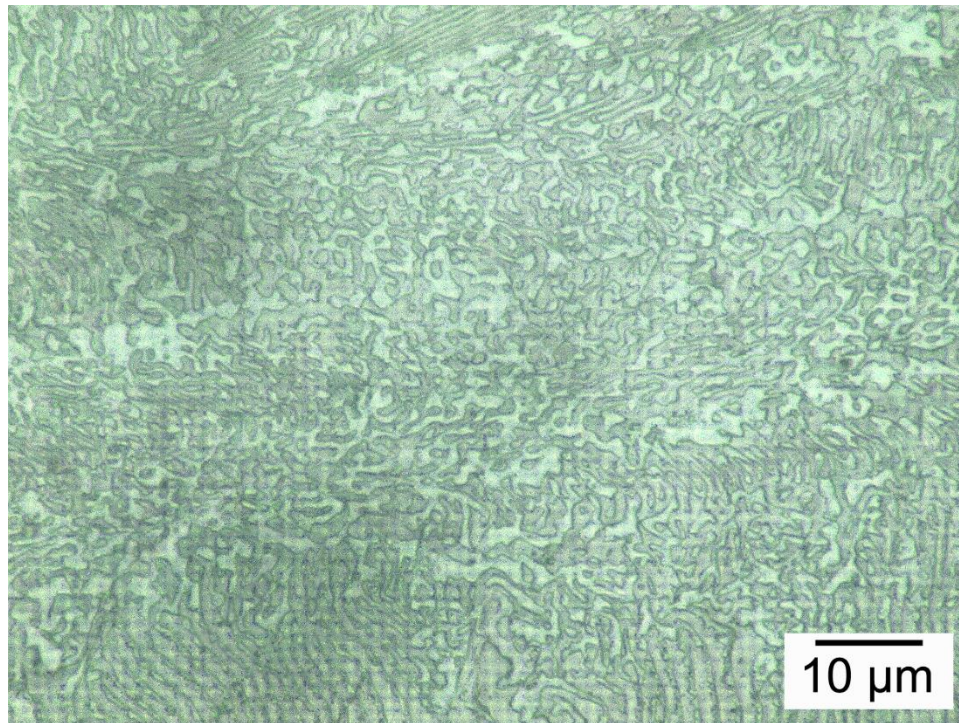


Figure 19: Optical micrograph of EC sample solidified in a graphite mold.

4.2.4. Solidification in copper molds

Copper bears high thermal conductivity [57], which allowed for a solidifying sample in copper molds to lose heat rapidly. In this set of experiments, the molten alloy near 800°C was poured into a pure copper mold (Figure 20). A copper sheet at

room temperature and bearing similar dimensions was placed onto the mold to reduce the solidification time and obtain a fine microstructure. Therefore, in place of a cylindrical mold, a shallow copper mold was used. Here the solidified specimen was a thin sheet with a more homogeneous growth. This enhanced the possibility of producing uniform porosity and ligament sizes after selective dissolution.

To secure microstructure stability, we used an annealing treatment, as described in Methodology section. Hence, in the alloy only two phases were present: a primary Al phase and a eutectic mixture of aluminum and Al_2Cu .

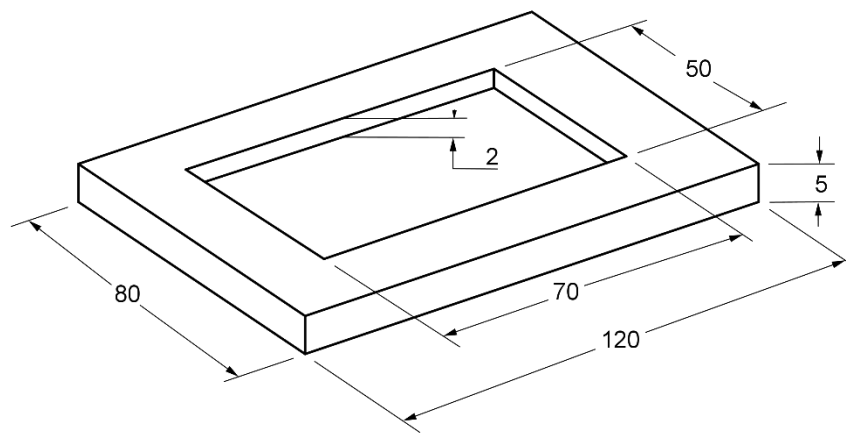


Figure 20: Mold used in solidification process, all units in mm.

As expected, the EC sample shows a lamellar structure, as one can see in Figure 21, which presents the specimen after corrosion. This was completed in a 10 vol% NaOH aqueous solution for 24 hours. Without corrosion the microstructure was not clearly visible in the SEM images. An overall view of the microstructure is depicted in this SEM image, where different local solidification directions can be observed, leading to an equiaxed structure. This image also demonstrates that this method of solidification is more effective (in terms of uniformity and refinement) than the ones

already described in sections 4.2.2 and 4.2.3. Consequently, after annealing, the precursor microstructure still remains fine, and pores are not apparent.

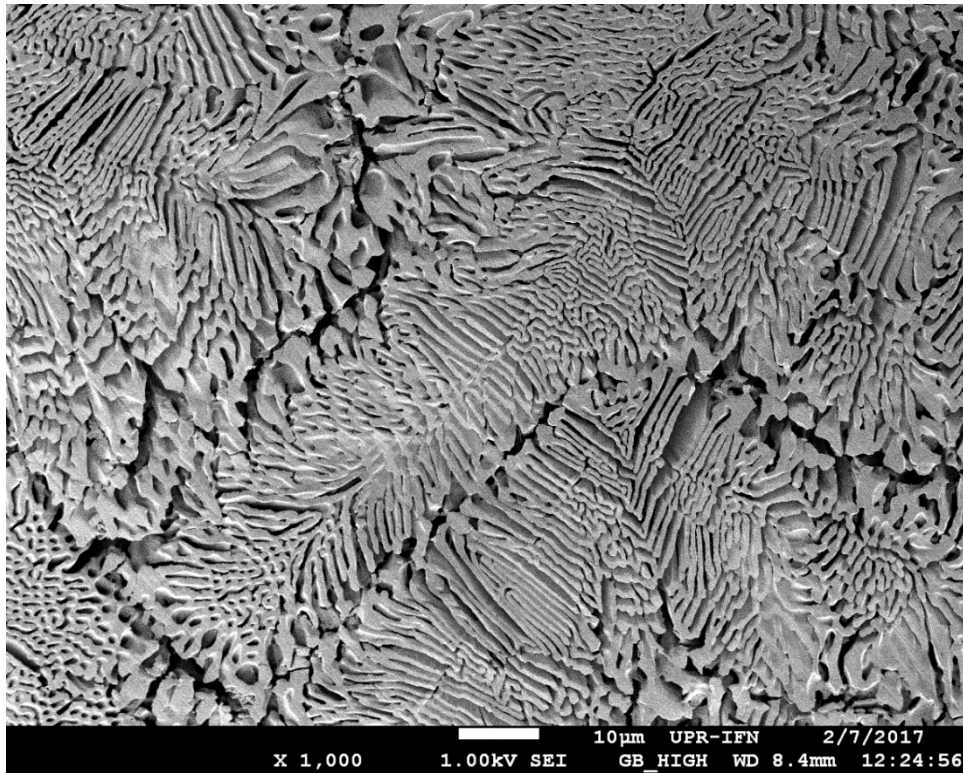


Figure 21: SEM image of an EC sample solidified in a copper mold and corroded for 24 hours in 10 vol% NaOH aqueous solution.

HC-1 samples do not show dendritic formation as one would have expected from the equilibrium phase diagram. This composition is too close to the eutectic composition, i.e. in the coupled zone, where the type of solidification (assuming high undercooling in this research) can lead to the eutectic cells formation. This could occur because the eutectic grows more rapidly than dendrites of Al_2Cu phase [58].

Figure 23 shows a sample of Al-Cu with hypereutectic composition with proeutectic Al_2Cu . This is surrounded by eutectic regions. Therefore, in this sample there are regions with dendrites of different sizes, those of the eutectic region and those of the primary formation regions.

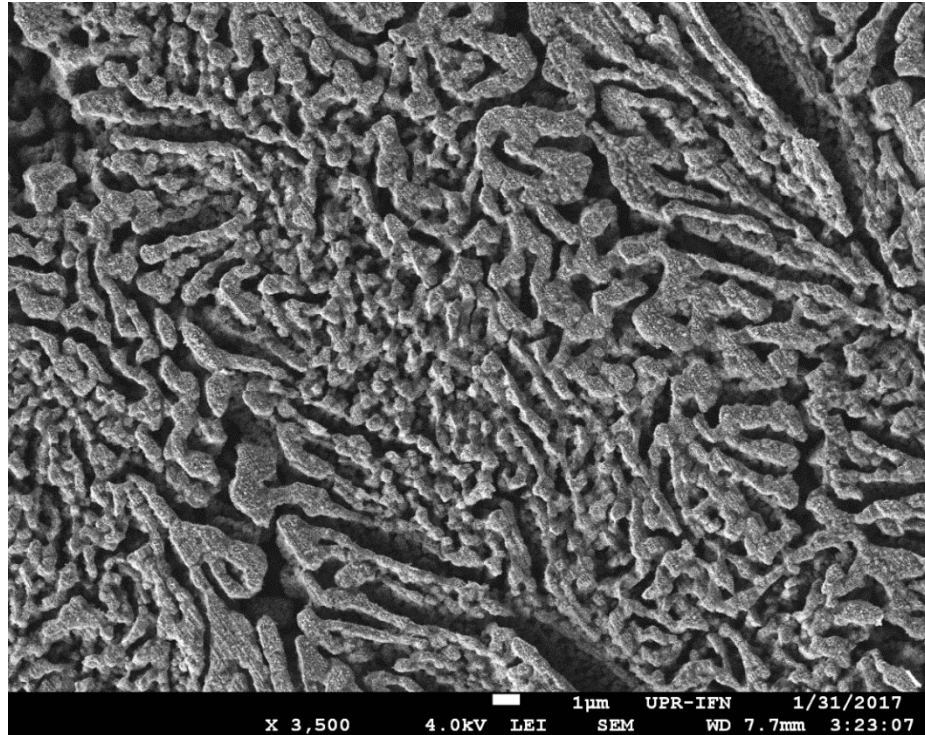


Figure 22: SEM image of a HC-1 sample solidified in a copper mold and after corroded for 24 hours in 10 vol% NaOH aqueous solution.

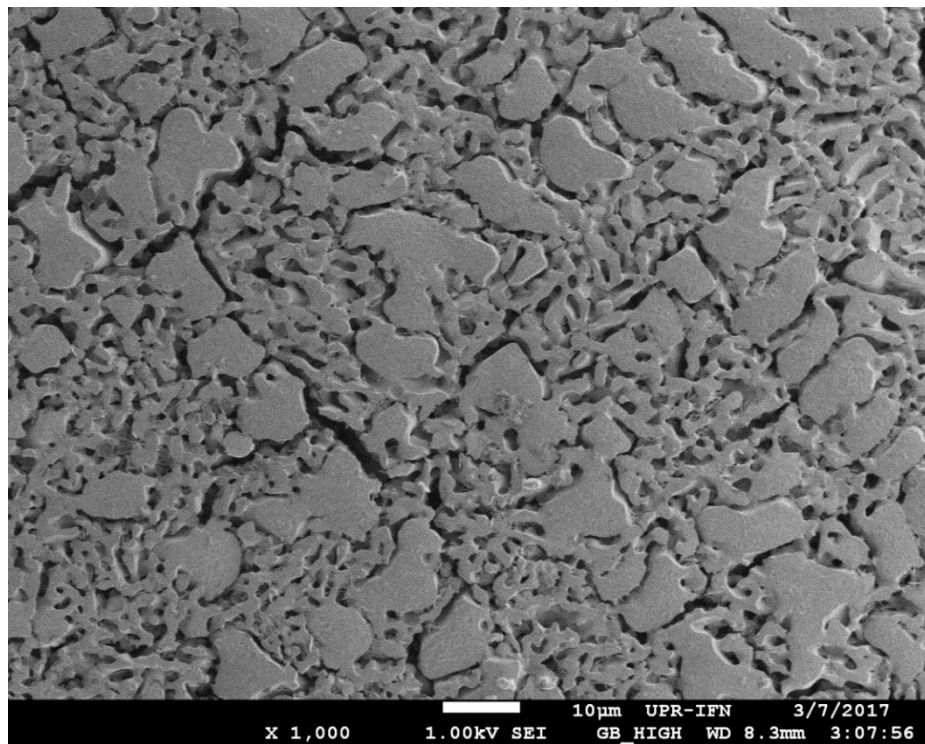


Figure 23: SEM image of a HC-2 sample solidified in a copper mold and after corroded for 24 hours in 10 vol% NaOH aqueous solution.

4.3. ANNEALING EFFECT

Due to the solidification method used, likely the diffusion process was affected, causing the microstructure not to be homogeneous. To enhance diffusion and stabilize the microstructure, a 400°C annealing was carried out for several time periods. This procedure caused the directional solidification microstructure to be lost. In effect, according to the literature, the type of microstructure observed is susceptible to fragmentation, spheroidization, and even coalescence of eutectic particles [59]. These process can be caused by Oswald ripening, where diffusion occurs from high to low curvature phases [60]. The spheroidization has been studied in aluminum-silicon systems with aggregates of sodium and strontium [61]. Also in aluminum-nickel alloys, the thermal treatment can lead to globularization in eutectic regions. In this system, Belov et al. discovered that when there is a colony structure, the globularization occurs more easily than other structures [62].

Annealing requires high temperatures to activate the diffusion. At the same time the Oswald ripening mechanism is activated as well. The samples with directional solidification present high variations in curvature between the central and external regions of each colony. These great differences favor diffusion, because the driving force for ripening process increases with high curvature differences, causing the disappearance of the smaller regions. Figure 24 shows a magnified area of the longitudinal section of a eutectic sample solidified directionally. On the right of the image, finer formations are noted. On the contrary, on the left of this image a perimeter of a colony is observed where the morphology presents bigger formations. Microstructural alterations of the directionally solidified samples are detected after a 4 hour annealing (Figure 25). Most lamellae were destroyed or fragmented.

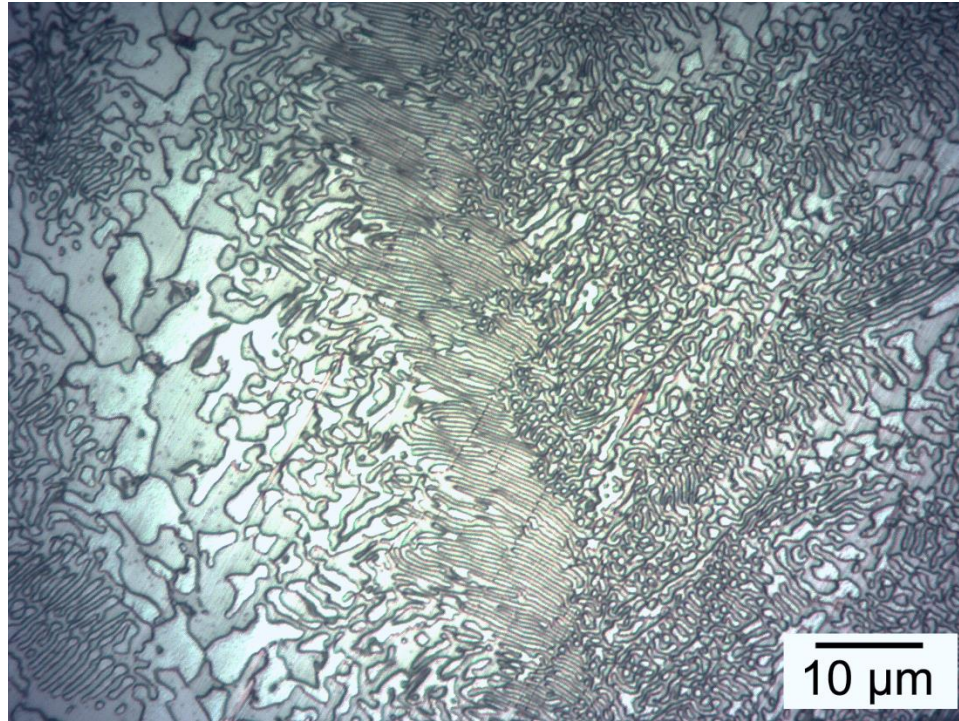


Figure 24: Optical micrograph of Al-Cu eutectic alloy directionally solidified, longitudinal section view magnified more than in Figure 17.

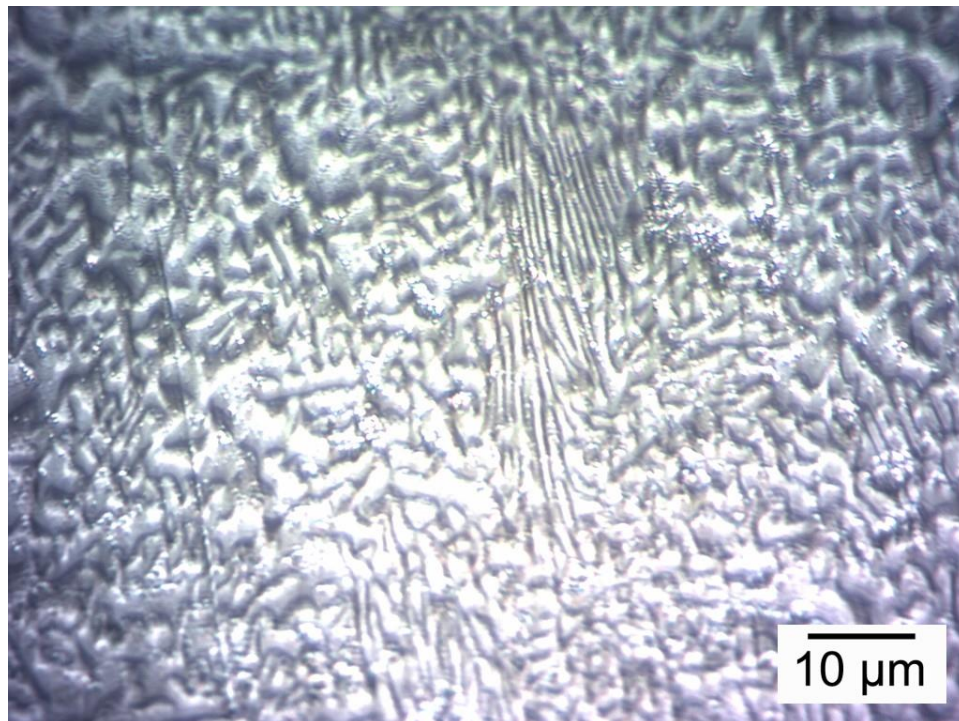


Figure 25: Optical micrograph of eutectic Al-Cu directionally solidified after annealing for 4 hours.

After the 24 hour annealing, the as cast microstructure was completely modified. Now the morphology is quite uniform without eutectic lamellas (Figure 26). The microstructural shape variations only occurred in samples with directional solidification. In samples solidified in copper molds, the annealing did not alter the overall structure morphology since these samples present an interface between phases with much less curvature than the eutectic colonies. In other words, smooth planar surfaces avoid the fragmentation during heat treatments even at temperatures near the equilibrium solidus line [59].

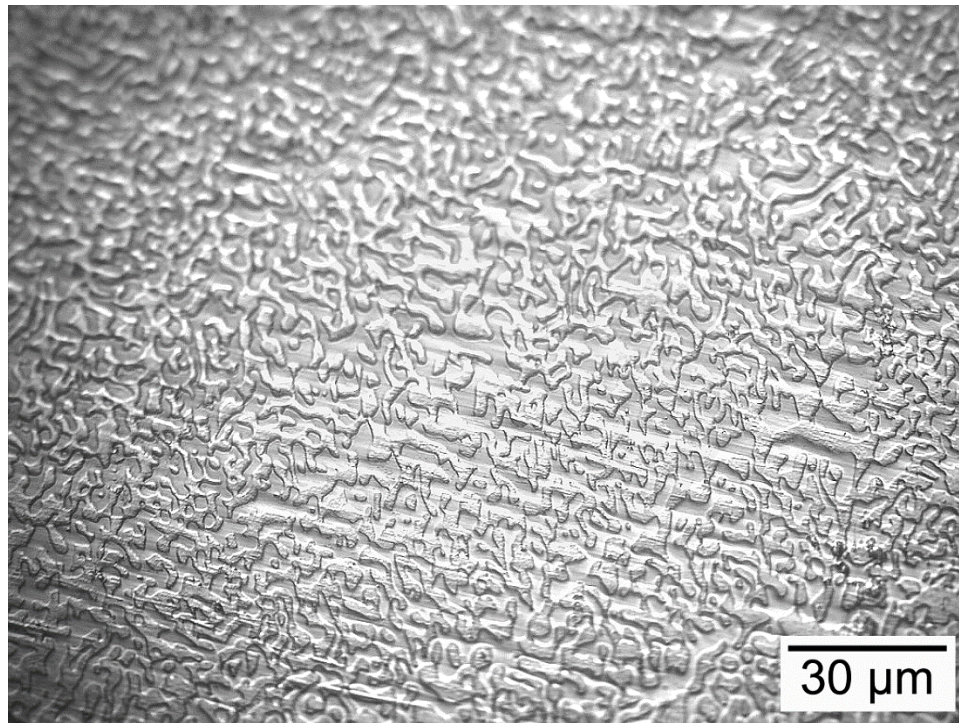


Figure 26: Optical micrograph of EC directionally solidified and annealed at 400°C for 24 hours.

5. SELECTIVE DISSOLUTION PROCESS

In this research segment we tested corrosion by sodium-hydroxide (NaOH) and nitric-acid (HNO₃) to discover whether these chemicals compounds were effective in removing the Al phase. This process was carried out by free corrosion because it is inexpensive and relatively simple.

There are several factors that affect this corrosion type, such as temperature, pressure, electrolyte concentration, and exposure time. Thus, the corrosion procedure took place at room temperature and atmospheric pressure to expedite the fabrication process for this material. Therefore, only the effects of electrolyte concentration and exposure time on the sample structure were studied.

5.1. FREE CORROSION OF DIRECTIONALLY SOLIDIFIED SAMPLES

Free corrosion in NaOH was performed at different hydroxide aqueous solution concentrations, namely 1, 10 and 25 vol%. Table 3 presents a summary of the results.

Table 3: Observed reactions for samples directionally solidified in NaOH at different concentrations.

NaOH Concentration	Corrosion observation
1 vol%	Slow reaction, selective dissolution at long time.
10 vol%	Fast corrosion, selective dissolution at controlled periods of time.

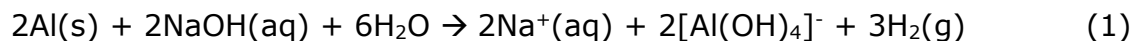
25 vol%

Very fast and aggressive reaction, no selective dissolution.

The 25 vol% aqueous solution completely dissolved the sample, which was destroyed by the electrolyte in a relatively short time. The 1 vol% NaOH concentration produced a similar result as 10 vol% but at a much longer time. Optical microscopy observations demonstrated that selective dissolution of the Al phase became apparent. Since the selective dissolution process using a 1 vol% NaOH solution took too long (more than 48 hours), thereafter the study focused only on the 10 vol% concentration.

Under these conditions, apparent selective dissolution was achieved with controlled exposure time. This meant that the sample must be removed from the solution when chemical reactions were still occurring; otherwise, the sample would be fully dissolved by the electrolyte, as in the case of the 25% solution.

The samples prepared following the procedure in section **3.3** were subject to a treatment in 100 ml of 10 vol% NaOH aqueous solution. This concentration allowed maintaining a stable reaction rate. This reaction is presented in Equation (1):



According to this reaction, tetrahydroxyluminate ($[\text{Al(OH)}_4]^-$), ionic sodium, and hydrogen gas are the reaction products. Hydrogen is responsible for the bubble formation, which has been used to monitor visually the chemical reaction progress.

5.1.1. Samples without annealing

The samples exposed for 4 hours to the corrosion medium did not show microstructural variations, as revealed by Figure 27. Likely, selective dissolution occurred as the intermetallic phase remained. In other words, Al_2Cu did not react with the NaOH solution. Figure 27 shows that the colony structure of a lamellar eutectic achieved by directional solidification was preserved when compared with the unetched microstructure in Figure 18, i.e. before corrosion.

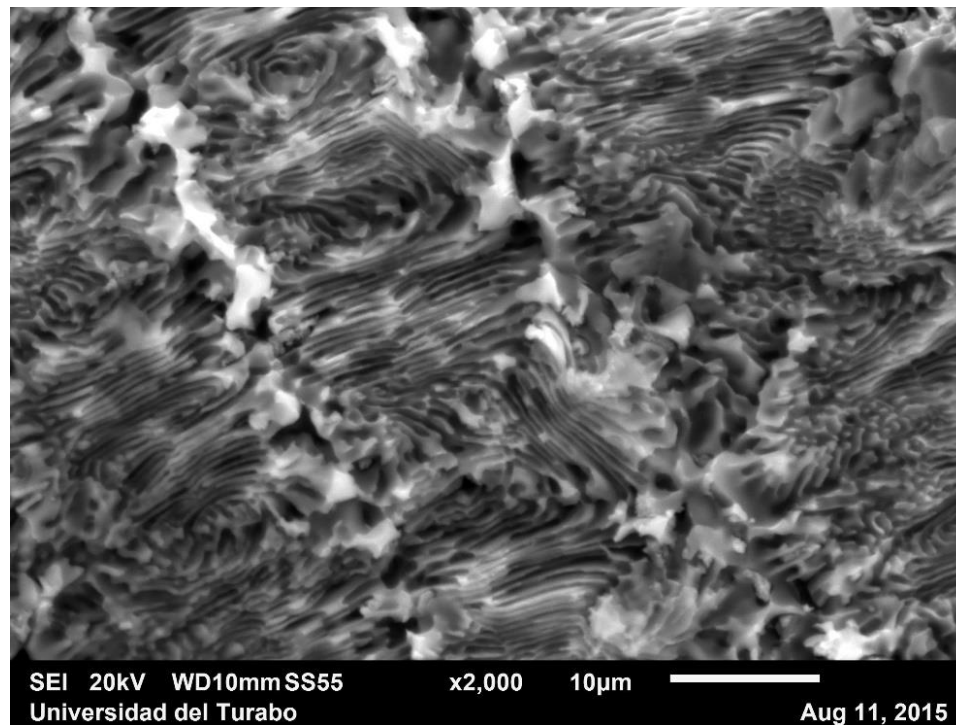


Figure 27: SEM image of Al-Cu eutectic directionally solidified and corroded in 10 vol% NaOH aqueous solution for 4 hours.

Figure 28 shows the lamellar structure of a center of a colony formed by directional solidification. Pores of approximately 400 nm were obtained. However, this pore size can vary depending on the local thermal gradient and local solidification

time. In Figure 29 we observe the perimeter of an eutectic colony in which voids of around 2 μm are much larger than those present in interlamellar regions. These SEM images demonstrate that 4 hours sufficed to achieve selective dissolution using a 10 vol% NaOH solution. Thereupon, the intermetallic phase would begin to react with NaOH. Alternatively, those ligaments could detach due to brittleness upon removal of mass, as indicated in Figure 30.

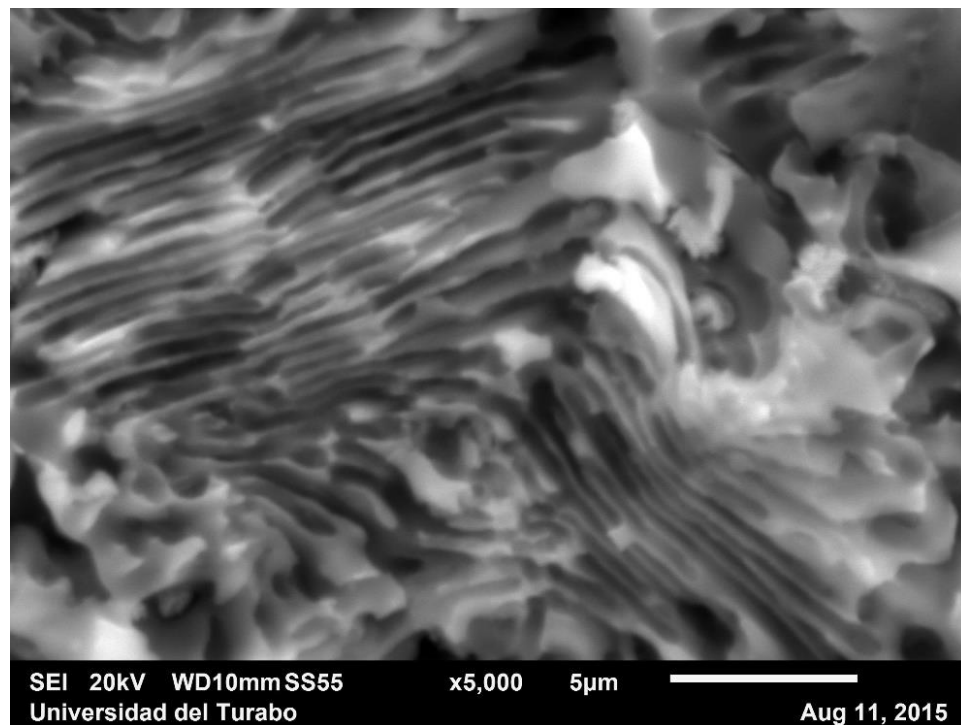


Figure 28: SEM image of Al-Cu eutectic colony in a directionally solidified specimen corroded in 10 vol% NaOH aqueous solution for 4 hours.

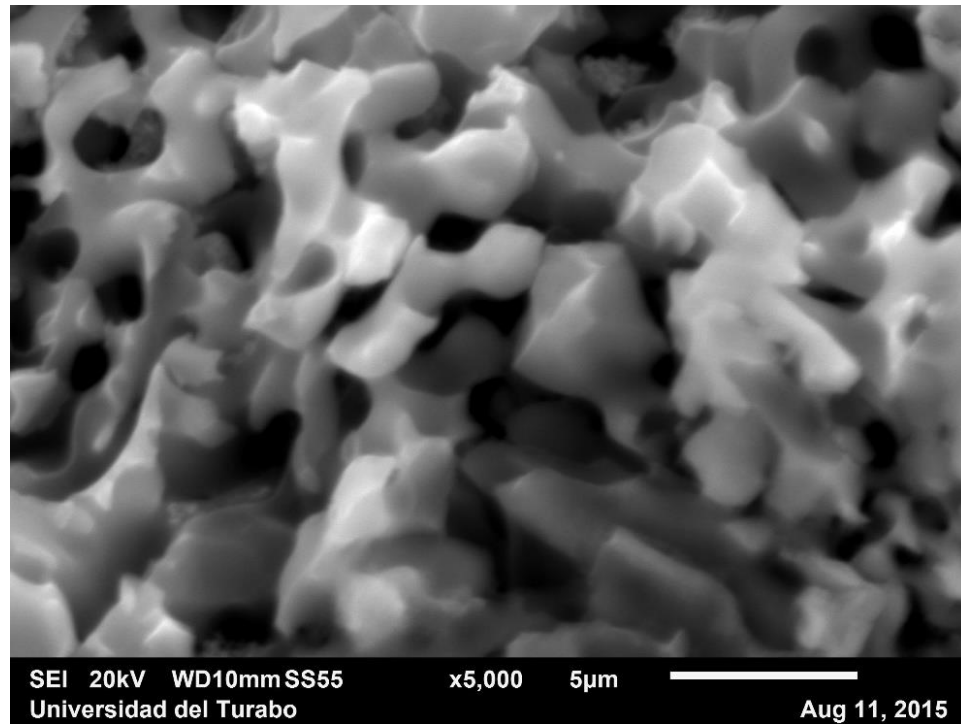


Figure 29: SEM image of the perimeter of Al-Cu eutectic colony in a directionally solidified specimen corroded in 10 vol% NaOH aqueous solution for 4 hours.

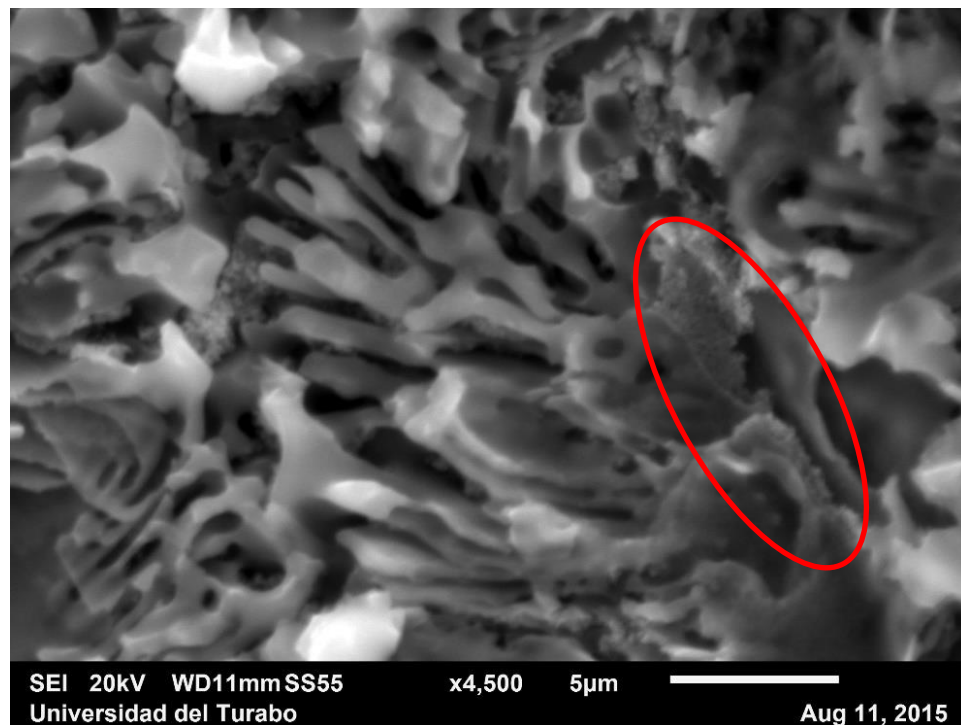


Figure 30: SEM image of a ligament detachment of in a eutectic Al-Cu specimen directionally solidified and corroded.

5.1.2. Annealed samples

The directionally solidified samples were annealed and then corroded under the same conditions as the samples without annealing. However, the exposure time to the corrosive medium was shorter in these samples, since at 4 hours upon corrosion, significant detachment of the intermetallic phase fragments occurred. This phase did not react initially with NaOH. This process may occur because the annealing caused a microstructural change, in which likely there is not an interconnected ligament network. Figure 31 shows a sample corroded for one hour and Figure 32, a magnified area of the same sample. These photographs suggest selective dissolution of the Al phase, although there was no improvement with respect to the samples without annealing, in which, the average pore size is smaller.

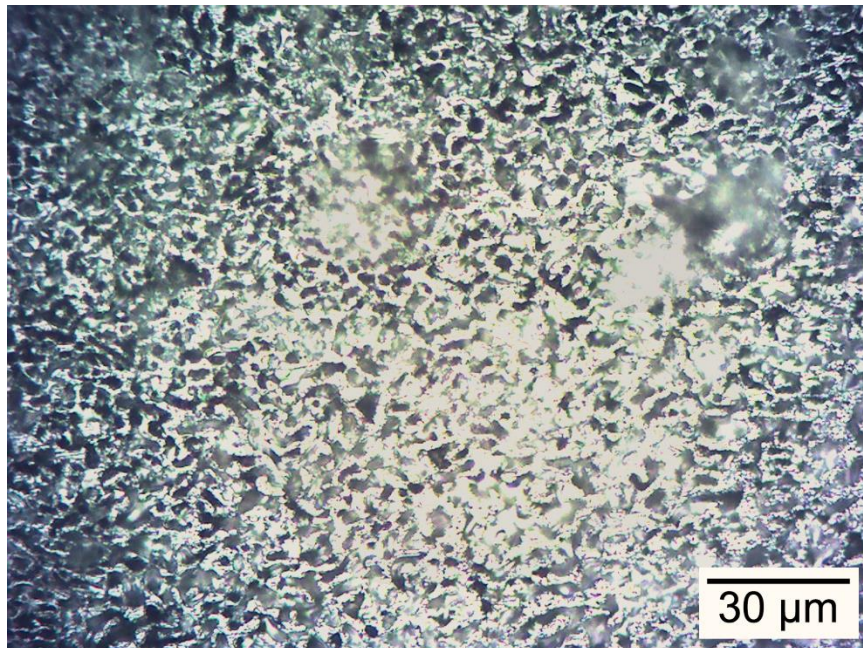


Figure 31: Optical micrograph of an EC sample corroded by 1 hour in NaOH (magnified 50X)

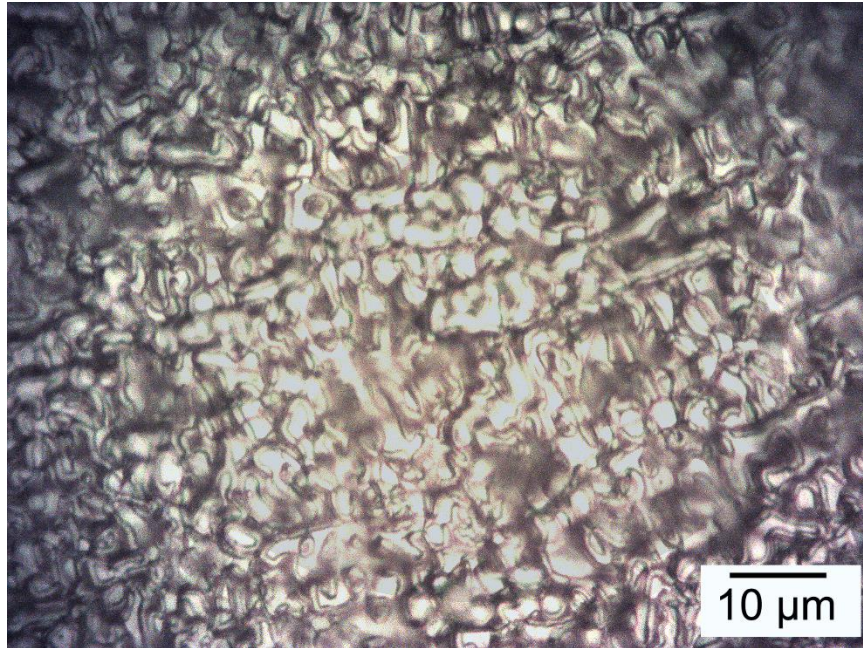


Figure 32: Optical micrograph of an Al-Cu eutectic sample corroded by 1 hour in NaOH with higher magnification than Figure 31.

5.2. SELECTIVE DISSOLUTION OF SAMPLES SOLIDIFIED IN COPPER MOLDS

The results of the directionally solidified samples demonstrate that the 10 vol% NaOH aqueous solution is effective for this process. Consequently, the samples solidified in copper molds were corroded with this solution concentration. The chemical reaction produced is the same as that described in section 5.1, in which tetrahydroxyluminate, $\text{Na}^+(\text{aq})$, and hydrogen gas are the reaction products. Again, the evolution of hydrogen gas has been an indicator of ongoing corrosion in the sample. Thus, if this bubble formation is not exhibited after 24 hours corrosion one can assume that the reaction stopped or, at least, slowed down significantly. At the end of this process the sample maintained the initial dimensions with enough

structural integrity (no crumbling). Change in the sample coloration was observed, now brown copper (as seen in Figure 33), and the surface of the sample is still reflective as before corroding.



Figure 33: Photographs of a HC-2 sample, a) before and b) after corrosion in 10 vol% NaOH for 24 hours.

This technique is assumed to lead to selective dissolution, in which the NaOH reacts with Al, and the θ phase remains as an interconnected network of ligaments. Now, the process does not depend on controlling the exposure time. Instead, the samples remained submerged during noticeable bubble evolution. Thus, the process was reproducible.

The selective dissolution was carried out on the three Al-Cu alloy compositions described in section 3.2. The three different compositions presented similar behavior during corrosion, starting with a relatively fast reaction until dissolution stopped before 24 hours.

5.2.1. SEM study

From the SEM images, the porosity of the samples was determined, as well as the pore and ligament size after corrosion. The porosity analysis was performed in

MATLAB®, whereas pores and ligaments size were measured using ImageJ [63]. For this characterization, several images were considered in order to have reliable statistics.

Sample porosity

Figure 34 and Figure 35 reveal the surface of the samples for the HC-2 and EC respectively. A finer grain is observed in the EC sample than in the HC-2 sample, but they keep the same microstructure features. This causes the surface to turn rough leading to a larger surface area of the sample, more than expected. The specimens displayed this feature throughout the entire surface in the eutectic laminae in all three compositions.

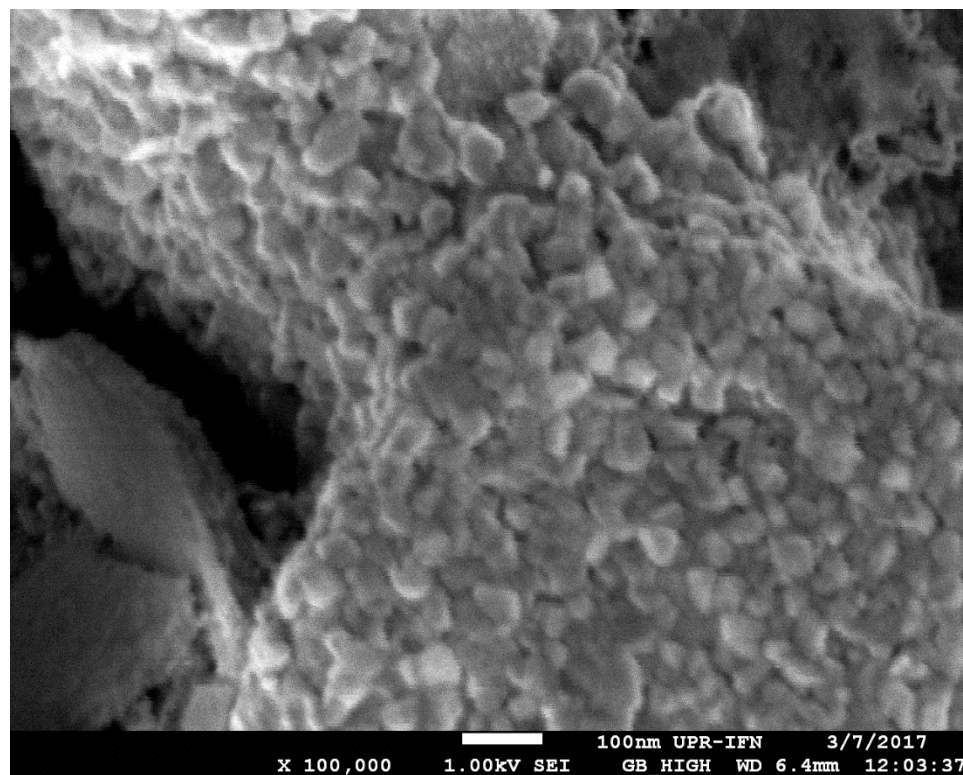


Figure 34: Surface of HC-2 sample after corrosion.

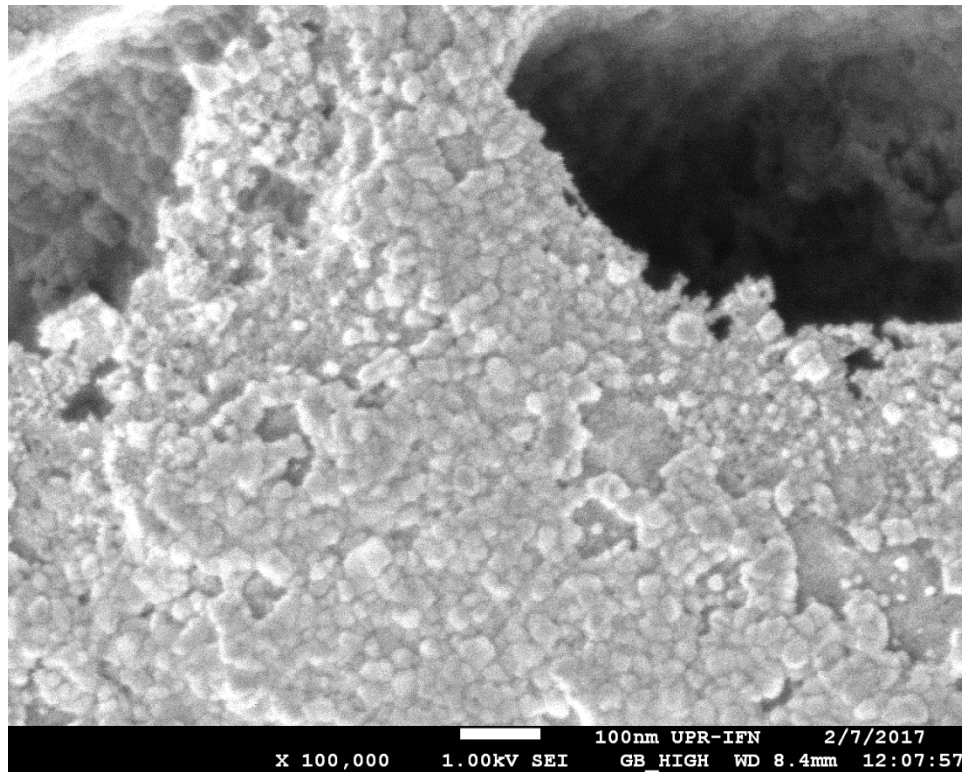


Figure 35: Surface of EC sample after corrosion.

The steps to measure the sample porosity are illustrated in Figure 36: a) original SEM photograph, b) elimination of areas that do not correspond to the observed cutting plane, c) conversion of the RGB image to binary image and inversion, where white areas correspond to pores, and d) boundaries of pores observed in the photograph. The MATLAB® program to perform this procedure is included in the Appendix.

The porosity analysis was performed on the SEM images at different magnifications and in all three compositions. This analysis revealed a porosity percentage of 51.3, 50.6 and 45.6% for EC, HC-1, and HC-2, respectively. These results show that the process removed more mass than expected compared to the information provided by the Al-Cu equilibrium diagram. This is particularly true for

the hypereutectic compositions, where the excess porous area is about 4.4%. For the EC there seems to be no significant excess, since it was expected to lose 50% of its volume, equivalent to the amount of α Al phase. The loss of mass can occur as a result of the solidification microstructure. Upon solidification, the high thermal gradient produced finer grains, i.e. numerous grain boundaries. Many atoms are not perfectly bonded to the crystalline structure, leading to a corrosion process that removed more atoms than expected during the selective dissolution.

Formation of solid precipitates during the annealing process is another important factor. During solidification, some Cu atoms can be dissolved in the primary phase of Al due to high cooling rates and they may form precipitates of the intermetallic phase upon annealing. These precipitates can remain isolated and when the corrosion takes place, those regions can fall into the electrolyte.

Image analysis allowed correlating the porous area measured with the porosity volume. In the same way, the pore boundaries could also be associated to the increase of surface area. When performing this calculation, the said area in all three compositions increased approximately 7 times compared with the initial area. However, this result assumes that the pore boundaries are perfectly defined; in other words, the surface appears smoother at a lower magnification, unlike that observed in Figure 34 and Figure 35, where the surface area is rough. For this reason, the increased area turns out to be smaller than expected. Measurements of this surface area using a Brunauer-Emmett-Teller (BET) surface area analyzer for EC, resulted in an area close to 0.41 m² for 3×2×10 mm samples; this represents a surface area more than 3,600 times larger than the initial area.

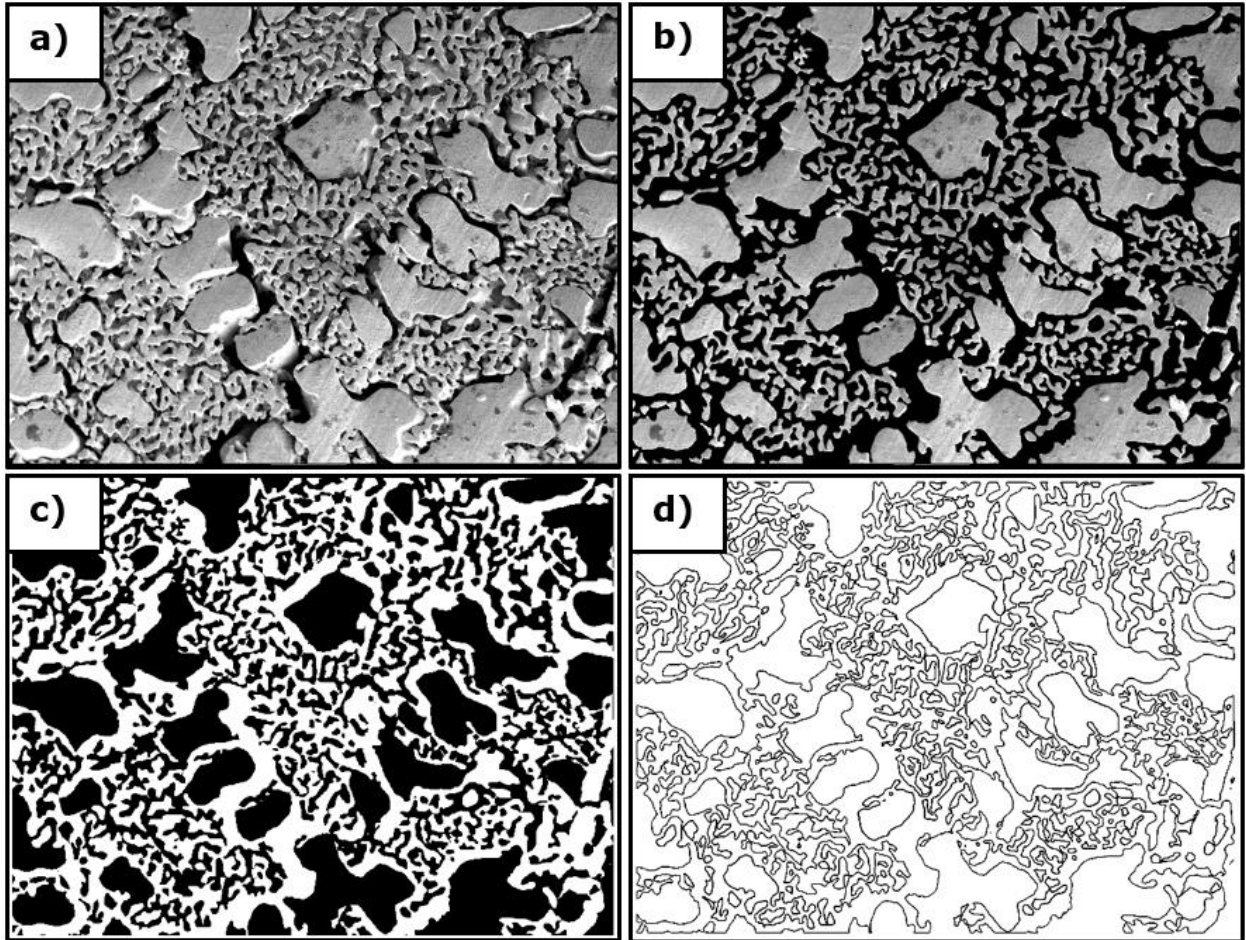


Figure 36: Example of steps for percent porosity estimation of one sample, a) original SEM photograph, b) elimination of areas that do not correspond to the observed cutting plane, c) conversion of the RGB image to binary image and inversion, where white areas correspond to pores, and d) boundaries of pores observed in the photograph.

Pore and ligament size

Using ImageJ image analyzer allowed determining the pore and ligament size of the three said compositions. Several images and at least 600 values of pores and ligaments for each composition were taken into consideration. Figure 37, Figure 38, and Figure 39 are examples of typical photographs used in this measurement, where one can observe the differences in the microstructure with large eutectic regions. Only the HC-2 specimen presents proeutectic θ dendritic formation.

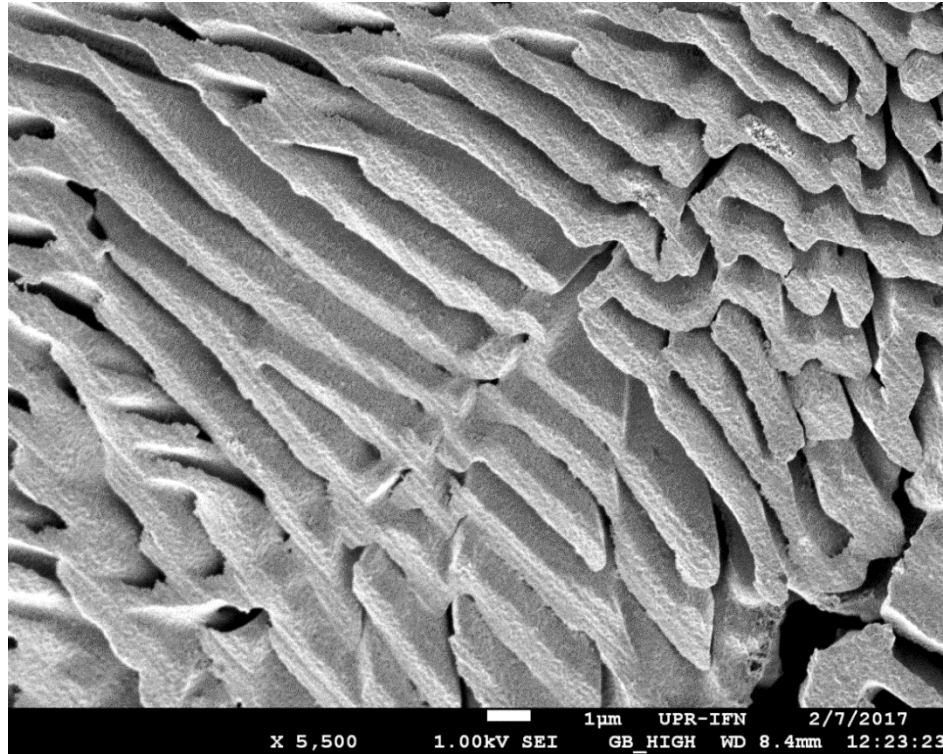


Figure 37: SEM image of the EC sample corroded to determine pore and ligament size.

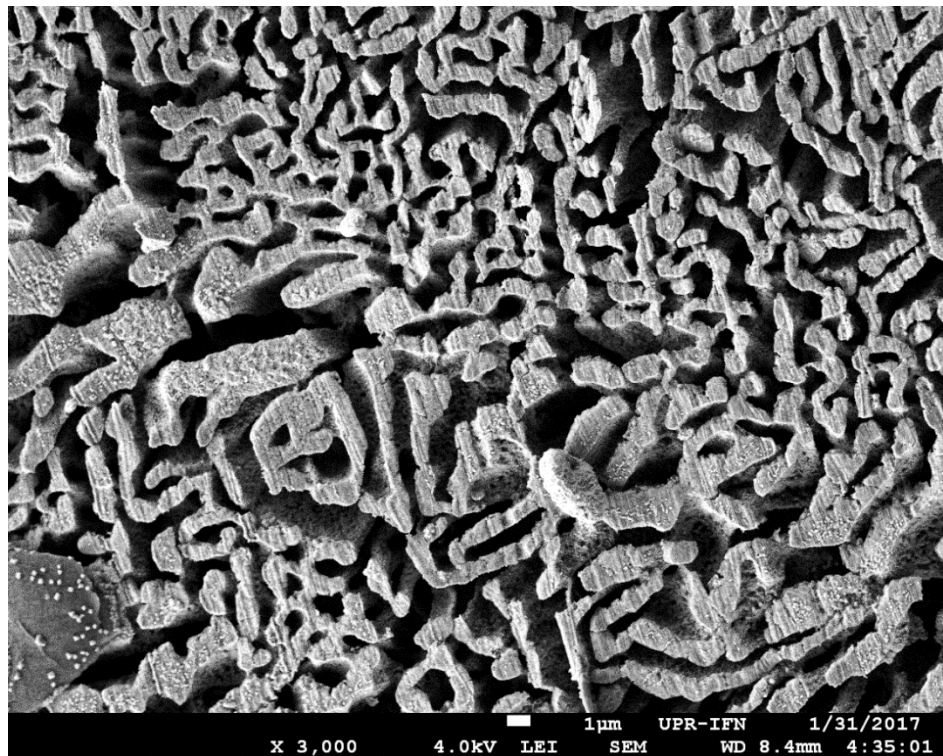


Figure 38: SEM image of the HC-1 sample corroded to determine pore and ligament size.

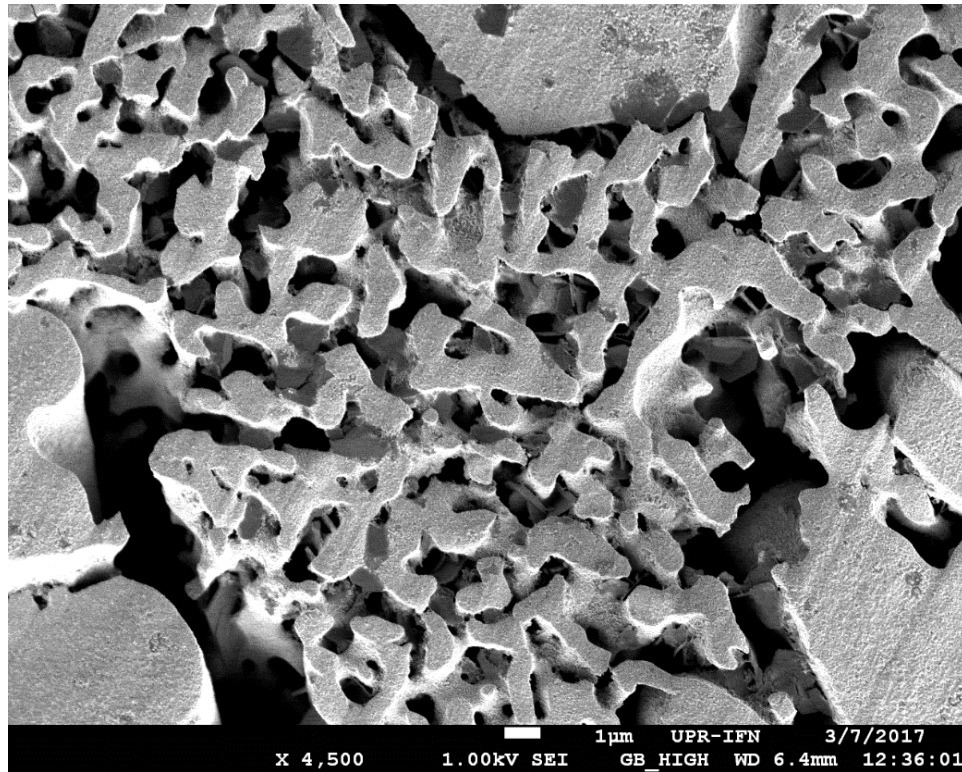


Figure 39: SEM image of the HC-2 sample corroded to determine pore and ligament size.

Using the values obtained from ImageJ, the graphs in Figure 40 and Figure 41, as well as Table 4 were produced. Figure 40 is a boxplot of pore sizes by composition. Smaller pore size is highlighted in the HC-1 specimen with many more values in the first two quartiles. This occurred because the microstructure of HC-1 sample does not show a dendritic formation. Instead, there are differentiated regions in which the laminae thicknesses vary much; in some areas this is even finer than in the EC. The pore sizes in EC and HC-1 present a similar range of values. However, the dispersion is much higher in HC-2, as Table 4 shows. According to the phase diagram, HC-1 should have dendritic formations. Nevertheless, the solidification conditions did not allow the formation of these (as already shown in section 4.2.4), causing a eutectic microstructure to appear throughout the entire sample. Therefore, the growth of the

lamellas was not uniform as in EC samples producing the high dispersion observed in the pore and ligament sizes.

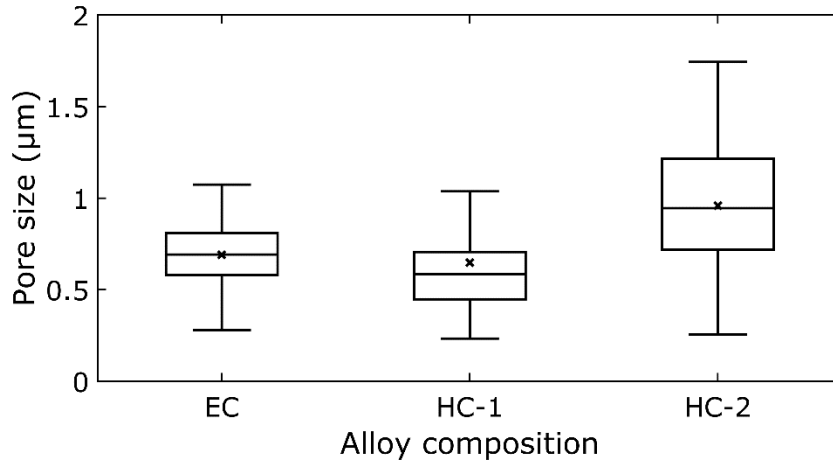


Figure 40: Box plot of pore size for the three compositions studied.

Table 4: Pore and ligament size measurements.

Type	Average size (nm)			Standard deviation (nm)		
	EC	HC-1	HC-2	EC	HC-1	HC-2
Pore	689.7	652.0	959.5	166.0	304.3	312.0
Ligament	433.4	584.5	1114.1	94.9	261.0	291.9

In Figure 41, the ligament sizes of the EC are uniform as the dispersion increases in the hypereutectic compositions as does the average value. In the HC-2 specimens, only the ligament sizes of the eutectic zones were considered.

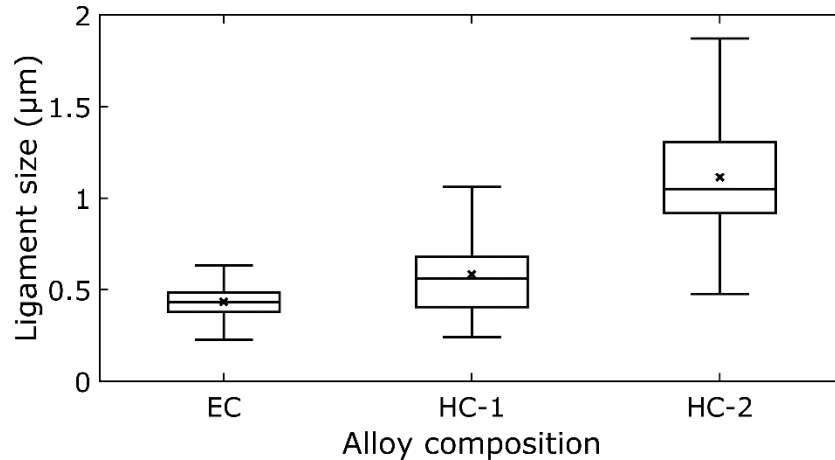


Figure 41: Box plot of ligament size for the three compositions studied.

The results of the porosity measurement suggest that the corroded eutectic alloy presented a larger surface area and more porosity than the hypereutectic compositions. Furthermore, the box plot of the ligament size revealed much less dispersion in the eutectic composition than in the hypereutectic specimens. The EC bears 50 vol% of both phases, which leads to similar lamellae thickness (eutectic Al₂Cu and eutectic Al) and, therefore, to a more homogeneous ligament size. These findings prove that the porosity can be controlled by the selection of the composition that would withstand the corrosion process.

As aforementioned, a nanoporous metal from a parent Al-Cu alloy could be obtained through selective dissolution by removing the Al phase. According to the literature, in dealloying Al-Cu alloys, pores and ligaments of smaller sizes (10-500 nm) have been attained [7]–[12]. In these studies, NPC was obtained via corroding the Al primary phase and also the intermetallic phase, i.e. Al₂Cu. As a result, pure nanoporous Cu was fabricated. At this point, we deem important to underscore that

this process differs from the selective solution, since dealloying involves diffusion of adatoms during the removal of one element (not one phase as in this research).

On the other hand, selective dissolution removes the Al phase but not Al atoms forming the intermetallic phase (Al_2Cu); in other words, dealloying of this phase did not take place in the presented corrosion process. This result can be further corroborated by observing the phase morphology in the SEM images. The retention of the Al_2Cu phase is further substantiated by the x-ray diffraction results. Additionally, free corrosion was used to achieve selective dissolution, which is much easier than the dealloying process where a specific applied electrical field is needed to create the most favorable dealloying conditions. Therefore, the proposed methodology is much less expensive, permitting to fabricate a new porous metal material.

All things considered, this research describes the fabrication of a low-cost metallic porous metallic material. The potential applications for this type of material are related to catalysis as well as sorbent material thanks to its large surface area. For instance, they can be used as a supporting framework for nanoporous high-performance sorbents [64]. The pore size and surface area define other specific applications of this novel material [65]. Further, the manufacturing process is quite adaptable to those applications, since by adjusting the solidification conditions one can modify the porosity and ligaments of the metallic framework. The scope of the present research could have been much expanded if we had had access to a three-dimensional x-ray tomography unit. However, we deem that the methodology used provides enough evidence of the effectiveness of the proposed selective dissolution.

The average pore and ligament sizes achieved in this research are 652 and 959 nm respectively among the three compositions studied. Although these values do not fall into the nanoscale classification, the dimensions of the pores and ligaments can be significantly reduced using a solidification method that further refines the microstructure, e.g. rapid solidification process. Again, the porosity obtained via selective dissolution depends directly on the as-cast microstructure.

5.2.2. Corrosion procedure

As mentioned, the objective of the selective dissolution is to eliminate one of the phases of the alloy. Furthermore, another goal is that the final porous material does not contain any other products resulting from the chemical reactions, which may occur during the dissolution process or after removing the sample from the electrolyte. For this reason, the selected method must produce a material without impurities. The new nanoporous material should contain only the metal interconnected by a network of ligaments.

During corrosion

As aforementioned, $\text{Al}(\text{OH})_4^-$ is one of the products of the reaction between the NaOH solution and the aluminum present in the sample. Ideally this product is dissolved by the electrolyte without creating another reaction. However, Counter et al [66] demonstrated that with a supersaturation of $\text{Al}(\text{OH})_4^-$ ion formation of aluminum hydroxide ($\text{Al}(\text{OH})_3$) nuclei can occur. These nuclei grow for hours (i.e. upon aging) and eventually become better defined structures observable at the nanometric scale. The $\text{Al}(\text{OH})_3$ formation is achieved through a supersaturation of

Al(OH)_4 ion, which can be reached at the sample surface during the corrosion process. The work by Counter et al. also demonstrated that the formation and growth of Al(OH)_3 removes the supersaturation of Al(OH)_4 ions allowing the reaction to continue.

The red circles in Figure 42 are some areas where there was possible Al(OH)_3 formation during the selective dissolution process. In this figure, formations with hexagonal shape can be observed. This geometry was studied by Schoen et al. [67] and through synthesis formed Al(OH)_3 with this particular shape. Figure 43 shows a magnified view of the same sample, in which formations of different sizes are observed. Corrosion was performed in a HC-2 sample for 24 hours and then passivated in ethanol to stop the chemical reaction. During the corrosion the sample was not aerated and the solution of NaOH remained motionless.

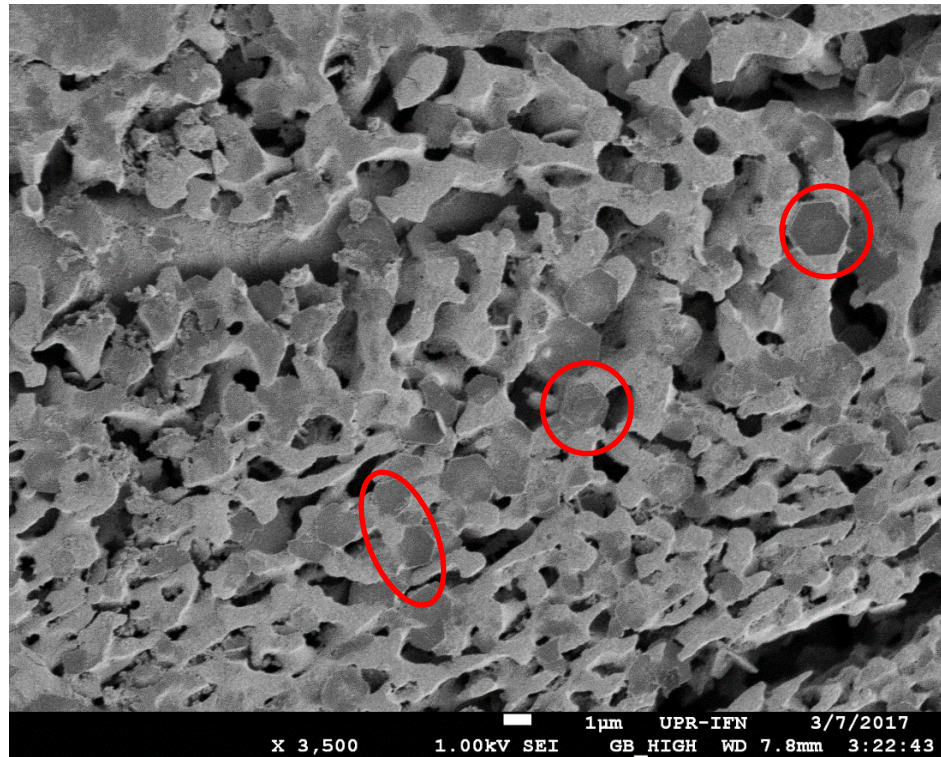


Figure 42: SEM image of a HC-2 sample with formation of aluminum hydroxide during selective dissolution.

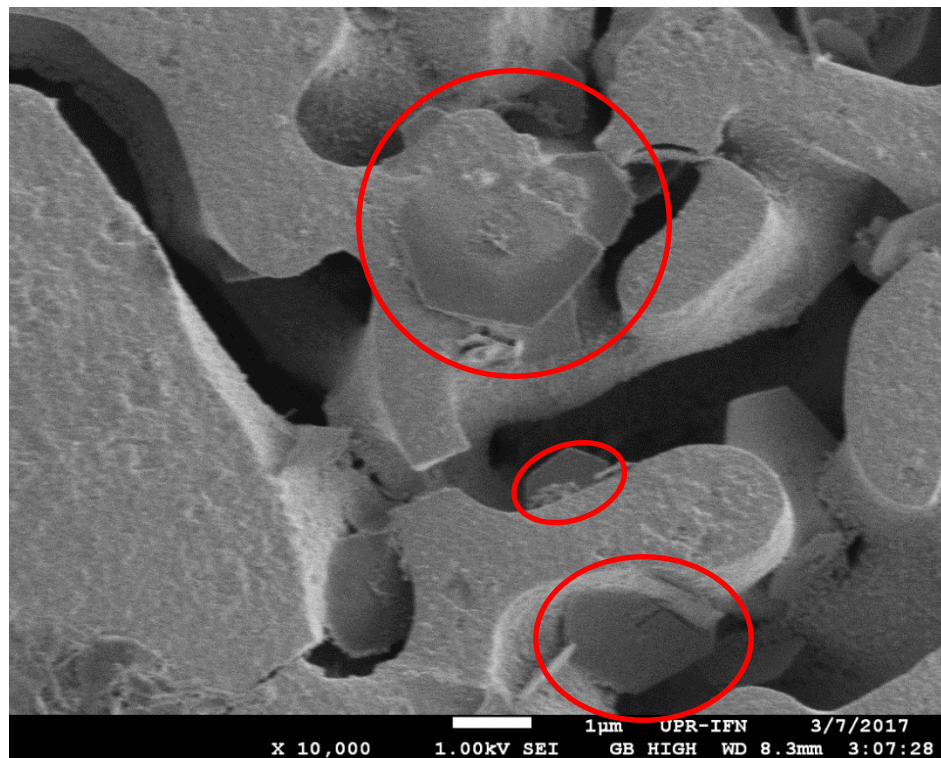


Figure 43: SEM image of a HC-2 sample with formation of aluminum hydroxide during selective dissolution (higher magnification than Figure 42).

To avoid supersaturation with $\text{Al}(\text{OH})_4$ ions and the subsequent formation of $\text{Al}(\text{OH})_3$, the NaOH solution must be in constant motion, which is achieved with a magnetic stirrer. When this method was used, no $\text{Al}(\text{OH})_3$ formation was observed in the SEM images.

After corrosion

When the sample in selective solution no longer displayed any bubble evolution, as aforementioned, we assumed that the reaction stopped. This occurs when the sample is still within the NaOH solution. Once the sample is removed from the electrolyte and comes in contact with air, other reactions could occur leading to the formation of aluminum oxide on the sample surface. For this reason, the sample must be passivated as soon as it is removed from the solution.

Figure 44 shows an EC sample that was not correctly passivated in ethanol and days later some aluminum oxide formed. This sample had been soaked in ethanol without stirring. Figure 45 shows a major formation of alumina, since the specimen was only placed in distilled water after the selective dissolution process.

To avoid the oxide formation, after corrosion the samples were placed in distilled water for 15 minutes and immediately in ethanol again for 15 minutes. It is important that when removing the samples from the NaOH solution, they should be in contact with air the shortest time possible. Additionally, both in distilled water and in ethanol, the sample must be placed in a sonication device; otherwise, this process will take much longer than indicated. Thus, if this method is used to stop the corrosion, the samples would not show oxide formation on their surface.

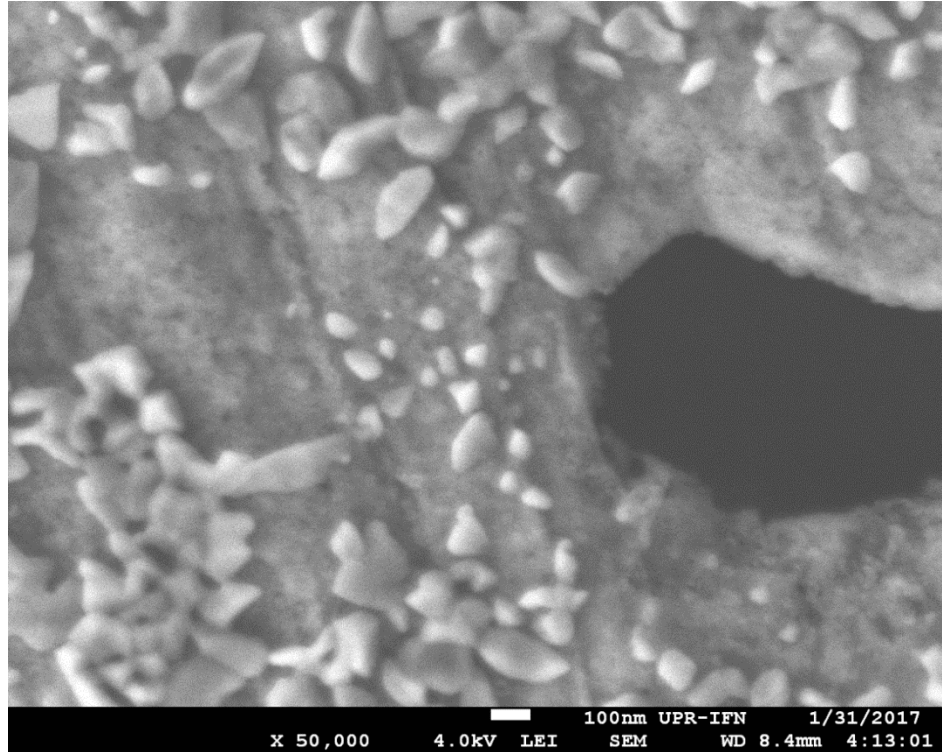


Figure 44: SEM image of EC sample with alumina formation due to incorrect treatment after corrosion.

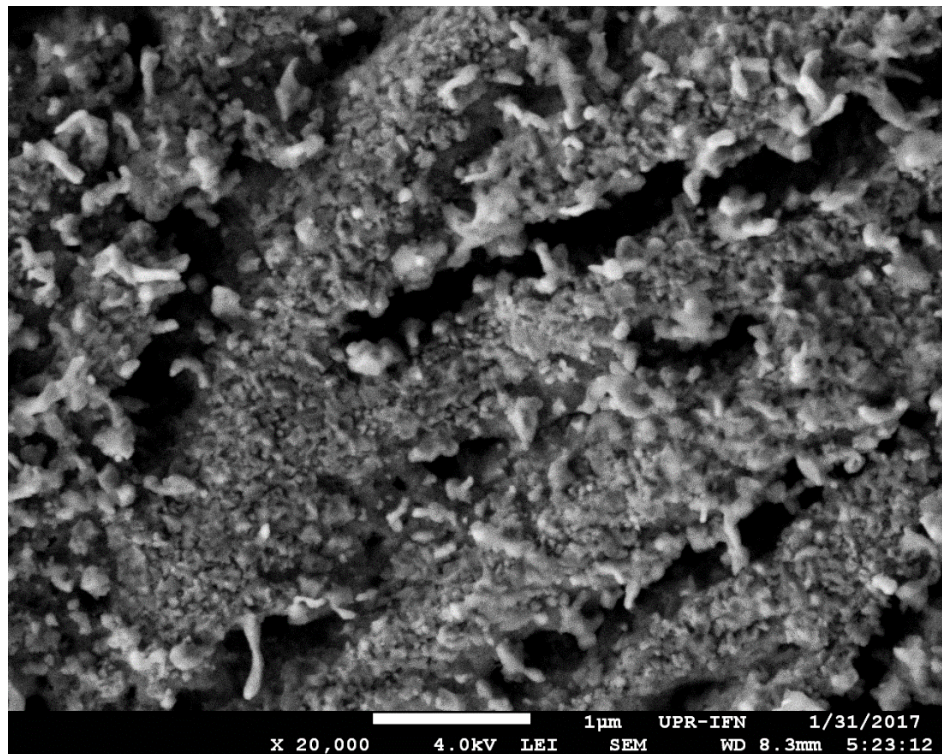


Figure 45: SEM image of aluminum oxide formation after selective dissolution in an EC sample.

5.2.3. X-ray diffraction results

The phases present in the material were studied via x-ray diffraction. In Al-Cu alloys, according to the pertinent equilibrium phase diagram, only Al and Al₂Cu should be present in a stable, uncontaminated specimen for compositions rich in aluminum. Therefore, through XRD the effectiveness of the selective dissolution process can be analyzed, as the selectively removed phase should not be present in the corresponding diffractogram. Hence, samples before and after corrosion were studied within the same 2θ range. This allowed characterizing the material assisted by a computer database containing the powder diffraction file [68]. This process was performed in the Match!(™) software [69]. Moreover, XRD shows whether another (unintended) phase formed from the reactions during and after the selective dissolution.

Figure 46 displays the XRD pattern obtained from an EC sample before selective dissolution. The phase peaks are labeled with the corresponding Miller indices of planes that reflected the x-ray beam and the respective phases.

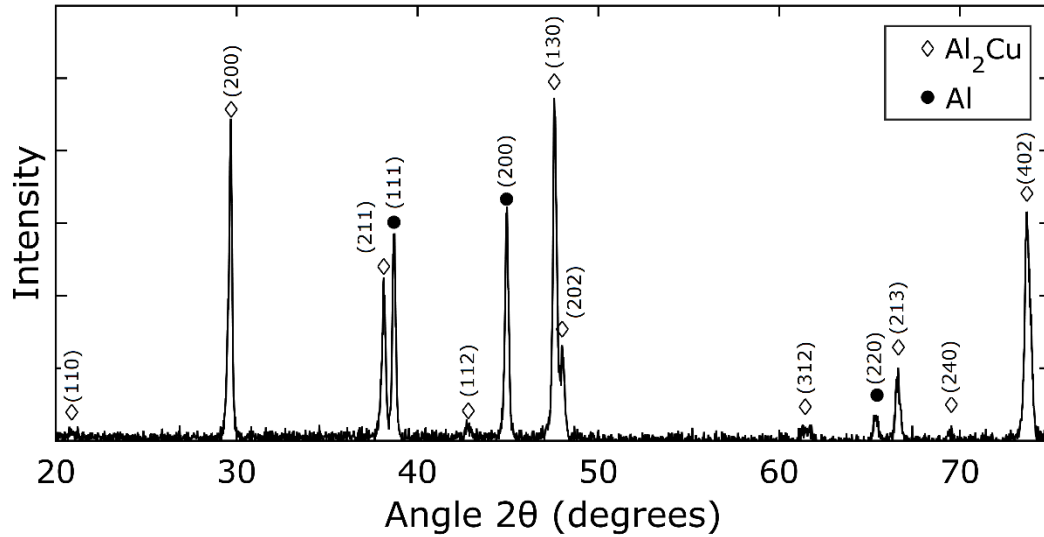


Figure 46: XRD diffraction pattern for EC sample uncorroded.

Figure 47 presents the diffractogram generated by an EC sample after selective dissolution. The peaks corresponding to the intermetallic phase are present, proving that the selective dissolution was effective. As mentioned in section 5.2.2, in order to make the entire process effective, after dissolution the corrosion process must be stopped. Otherwise, the sample could contain aluminum oxide (Figure 48) as a result of a stationary solution. and air exposure. As mentioned, these are undesirable oxides in the nanoporous material.

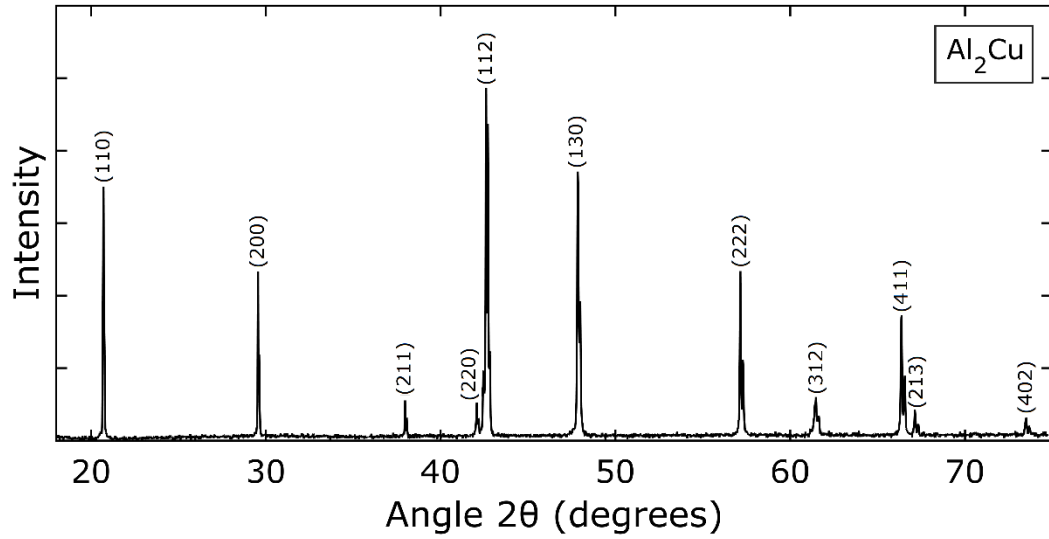


Figure 47: XRD diffraction pattern for corroded EC sample.

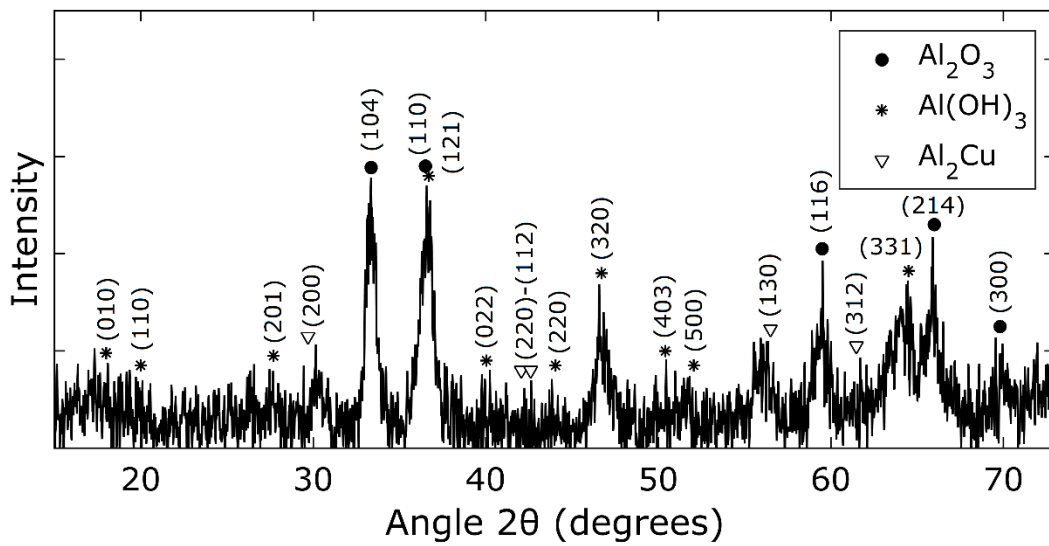


Figure 48: XRD diffraction pattern for EC sample corroded, without stirring during corrosion and aerated after that.

6. CONCLUSIONS AND SUGGESTIONS FOR FUTURE WORK

6.1. CONCLUSIONS

- Successful selective dissolution of the Al phase from a precursor Al-Cu alloy was achieved, proving the feasibility of manufacturing a porous metallic material made of an intermetallic phase. The pore sizes varied between 230 and 1,850 nm.
- The smaller average pore size (652 nm) were obtained in the Al-19.17 at% Cu specimen (named as hypereutectic composition 1), while larger ones (959.5 nm) were obtained in Al-20.80 at% Cu specimens (hypereutectic composition 2).
- Samples of eutectic composition present a greater uniformity and smaller ligaments size after the selective dissolution (433.4 nm). The ligaments for the hypereutectic compositions had a more variable and greater thickness. In addition, eutectic composition possesses the highest porosity value. This composition is the best one of those studied based on its high porosity, greater homogeneity, and, thus, final larger surface area.
- Solidification on copper sheets allowed a higher thermal gradient, causing finer microstructure. In addition, this solidification method avoided the formation of pores during this process.

- The 10 volume percent NaOH aqueous solution allowed a rapid chemical reaction and selective dissolution of the primary Al phase for the three compositions studied.
- During corrosion the electrolyte must be stirred lest the concentration of the resulting Al(OH)_4 ion increases on the sample surface. This avoids the Al(OH)_3 formation. After corrosion, the sample should be in contact with air the shortest time possible to avoid oxidation.
- The x-ray diffraction results validated the complete removal of aluminum phase present in the sample before the corrosion process, which was carried out for 24 hours.

6.2. SUGGESTIONS FOR FUTURE WORK

In order to understand better the process of selective dissolution in Al-Cu alloys, the author makes the following suggestions to improve the effectiveness in the fabrication of this porous metal:

- Study the corrosion rate. It is recommended to corrode samples of equal dimensions and weight at different periods of time. For each sample the initial and final area should be measured using the surface area analyzer apparatus. This method would allow reducing the amount of electrolyte needed for a given mass of the sample.
- Corrode the specimens using different electrical fields. Electrochemical corrosion would permit to determine if the process can be performed faster and with more control than through free corrosion.

- Using a grain refiner during melting. A finer microstructure would lead to smaller pores.

REFERENCES

- [1] J. Erlebacher, "Dealloying of Binary Alloys," in *Dekker Encyclopedia of Nanoscience and Nanotechnology, Second Edition - Six Volume Set (Print Version)*, CRC Press, 2004.
- [2] G. Q. Lu and X. S. Zhao, *Nanoporous Materials: Science and Engineering*, vol. 4. Imperial College Press, 2004.
- [3] Y. Ding and M. Chen, "Nanoporous Metals for Catalytic and Optical Applications," *MRS Bull.*, vol. 34, no. 08, pp. 569–576, Aug. 2009.
- [4] L. Chen, X. Lang, and M. Chen, "Dealloyed Nanoporous Metals," in *Nanoporous Materials*, CRC Press, 2013, pp. 125–182.
- [5] P. Schweitzer, *Fundamentals of Metallic Corrosion*, vol. 20067144. CRC Press, 2006.
- [6] T. Song, M. Yan, Z. Shi, A. Atrens, and M. Qian, "Creation of bimodal porous copper materials by an annealing-electrochemical dealloying approach," *Electrochim. Acta*, vol. 164, pp. 288–296, 2015.
- [7] S. Zhang *et al.*, "A three-dimensional tin-coated nanoporous copper for lithium-ion battery anodes," *J. Power Sources*, vol. 196, no. 16, pp. 6915–6919, 2011.
- [8] H. Jiang, J. Li, H. Geng, and Q. Wang, "Influence of cooling rate and addition of lanthanum and cerium on formation of nanoporous copper by chemical dealloying of Cu₁₅Al₈₅ alloy," *J. Rare Earths*, vol. 31, no. 11, pp. 1119–1124, 2013.
- [9] W. B. Liu, S. C. Zhang, N. Li, J. W. Zheng, and Y. L. Xing, "Influence of phase constituent and proportion in initial Al–Cu alloys on formation of monolithic nanoporous copper through chemical dealloying in an alkaline solution," *Corros. Sci.*, vol. 53, no. 2, pp. 809–814, 2011.
- [10] Z. Qi *et al.*, "Formation and Characterization of Monolithic Nanoporous Copper by Chemical Dealloying of Al–Cu Alloys," *J. Phys. Chem. C*, vol. 113, no. 16, pp. 6694–6698, Apr. 2009.
- [11] W. B. Liu, S. C. Zhang, N. Li, J. W. Zheng, and Y. L. Xing, "A facile one-pot route to fabricate nanoporous copper with controlled hierarchical pore size distributions through chemical dealloying of Al-Cu alloy in an alkaline solution," *Microporous Mesoporous Mater.*, vol. 138, pp. 1–7, 2011.
- [12] S. Nam, H. Jo, H. Choe, D. Ahn, and H. Choi, "Development of Nanoporous Copper Foams by Chemical Dealloying of Mechanically Alloyed Al - Cu Compounds," vol. 55, no. 9, pp. 1414–1418, 2014.
- [13] P. C. White, "Preparation of a raney catalyst surface," 1944.
- [14] M. Raney, "Method of preparing a catalytic material," 1925.
- [15] H. W. PICKERING and P. R. SWANN, "Electron Metallography of Chemical Attack Upon Some Alloys Susceptible to Stress Corrosion Cracking," *CORROSION*, vol. 19, no. 11, p. 373t–389t, Nov. 1963.
- [16] A. J. Forty, "Corrosion micromorphology of noble metal alloys and depletion gilding," *Nature*, vol. 282, no. 5739, pp. 597–598, Dec. 1979.
- [17] C. Leygraf *et al.*, "Selective dissolution and surface enrichment of alloy components of passivated Fe₁₈Cr and Fe₁₈Cr₃Mo single crystals," *Corros. Sci.*, vol. 19, no. 5, pp. 343–357, Jan. 1979.

- [18] N. Pertsov, V. Prokopenko, V. Zozulya, and M. Ivanov, "Processes of Ultradisperse Structures Self-Organization during Electrochemical Dealloying," in *Nanoscience: Colloidal and Interfacial Aspects*, CRC Press, 2010, pp. 515–522.
- [19] Y. Wang, J. Xu, and B. Wu, "Chloride ion effect and alloying effect on dealloying-induced formation of nanoporous AuPt alloy," *Appl. Surf. Sci.*, vol. 276, pp. 262–268, 2013.
- [20] X. Wang, Z. Qi, C. Zhao, W. Wang, and Z. Zhang, "Influence of Alloy Composition and Dealloying Solution on the Formation and Microstructure of Monolithic Nanoporous Silver through Chemical Dealloying of Al–Ag Alloys," *J. Phys. Chem. C*, vol. 113, no. 30, pp. 13139–13150, 2009.
- [21] Q. Kong, L. Lian, Y. Liu, J. Zhang, L. Wang, and W. Feng, "Bulk hierarchical nanoporous palladium prepared by dealloying PdAl alloys and its electrochemical properties," *Microporous Mesoporous Mater.*, vol. 208, pp. 152–159, 2015.
- [22] Z. Zhang, Y. Wang, Z. Qi, J. Lin, and X. Bian, "Nanoporous Gold Ribbons with Bimodal Channel Size Distributions by Chemical Dealloying of Al–Au Alloys," *J. Phys. Chem. C*, vol. 113, no. 4, pp. 1308–1314, 2009.
- [23] Q. Zhang, X. Wang, Z. Qi, Y. Wang, and Z. Zhang, "A benign route to fabricate nanoporous gold through electrochemical dealloying of Al–Au alloys in a neutral solution," *Electrochim. Acta*, vol. 54, pp. 6190–6198, 2009.
- [24] Y. Xu *et al.*, "A strategy for fabricating nanoporous gold films through chemical dealloying of electrochemically deposited Au–Sn alloys," *Nanotechnology*, vol. 25, no. 44, p. 445602, 2014.
- [25] W. J. Yeh and S. Chava, "Fabrication of metallic nanoporous films by dealloying," *J. Vac. Sci. Technol. B Microelectron. Nanom. Struct.*, vol. 27, no. 2, p. 923, 2009.
- [26] Y. Ding and J. Erlebacher, "Nanoporous Metals with Controlled Multimodal Pore Size Distribution," *J. Am. Chem. Soc.*, 2003.
- [27] X. Lang, A. Hirata, T. Fujita, and M. Chen, "Nanoporous metal/oxide hybrid electrodes for electrochemical supercapacitors," *Nat. Nanotechnol.*, vol. 6, no. 4, pp. 232–236, 2011.
- [28] A. Wittstock *et al.*, "Nanoporous gold: a new material for catalytic and sensor applications," *Phys. Chem. Chem. Phys.*, vol. 12, no. 40, p. 12919, Oct. 2010.
- [29] H. J. Qiu, J. L. Kang, P. Liu, a. Hirata, T. Fujita, and M. W. Chen, "Fabrication of large-scale nanoporous nickel with a tunable pore size for energy storage," *J. Power Sources*, vol. 247, pp. 896–905, 2014.
- [30] M. Liu *et al.*, "Electrochemical reactivity, surface composition and corrosion mechanisms of the complex metallic alloy Al₃Mg₂," *Corros. Sci.*, vol. 52, no. 2, pp. 562–578, 2010.
- [31] X. Wang, J. Sun, C. Zhang, T. Kou, and Z. Zhang, "On the microstructure, chemical composition, and porosity evolution of nanoporous alloy through successive dealloying of ternary Al–Pd–Au precursor," *J. Phys. Chem. C*, vol. 116, pp. 13271–13280, 2012.
- [32] X. Zhang, G. Li, S. Yang, X. Song, and Z. Sun, "Nanoporous CuO ribbons modified by Au nanoparticles through chemical dealloying and calcination for CO oxidation," *Microporous Mesoporous Mater.*, vol. 226, pp. 61–70, 2016.
- [33] F. M. Bayoumi and B. G. Ateya, "Formation of self-organized titania nano-tubes by dealloying and anodic oxidation," *Electrochem. commun.*, vol. 8, no. 1, pp. 38–44, 2006.
- [34] L.-Y. Chen, J.-S. Yu, T. Fujita, and M.-W. Chen, "Nanoporous Copper with Tunable Nanoporosity for SERS Applications," *Adv. Funct. Mater.*, vol. 19, no. 8, pp. 1221–1226, Apr. 2009.
- [35] R. Mao, S. Liang, X. Wang, Q. Yang, and B. Han, "Effect of preparation conditions on morphology and thermal stability of nanoporous copper," *Corros. Sci.*, vol. 60, pp. 231–237, Jul. 2012.
- [36] Y. Sun, Y. Ren, and K. Yang, "New preparation method of micron porous copper through physical vacuum dealloying of Cu–Zn alloys," *Mater. Lett.*, vol. 165, pp. 1–4, Feb. 2016.

- [37] T. Aburada, J. M. Fitz-Gerald, and J. R. Scully, "Synthesis of nanoporous copper by dealloying of Al-Cu-Mg amorphous alloys in acidic solution: The effect of nickel," *Corros. Sci.*, vol. 53, no. 5, pp. 1627–1632, 2011.
- [38] Z. Wang, J. Liu, C. Qin, L. Liu, W. Zhao, and A. Inoue, "Fabrication and new electrochemical properties of nanoporous Cu by dealloying amorphous Cu-Hf-Al alloys," *Intermetallics*, vol. 56, pp. 48–55, 2014.
- [39] E. G. Estremera-Pérez, "Fabrication and characterization of porous aluminum and zinc via selective dissolution of al-zn alloys," University of Puerto Rico at Mayagüez, 2013.
- [40] K. D. Sattler, *Handbook of nanophysics. 5, Functional nanomaterials*. CRC Press, 2011.
- [41] E. McCafferty, *Introduction to Corrosion Science*. Alexandria: Springer.
- [42] C. M. Forman and E. A. Verchot, "Practical Galvanic Series," 1967.
- [43] "Corrosion and oxidation [SubsTech]." [Online]. Available: http://www.substech.com/dokuwiki/doku.php?id=corrosion_and_oxidation. [Accessed: 03-Dec-2017].
- [44] "Stress Corrosion Cracking (3/4)." [Online]. Available: http://faculty.kfupm.edu.sa/ME/hussaini/Corrosion_Engineering/04.06.03.htm. [Accessed: 03-Dec-2017].
- [45] M. C. Flemings, *Solidification Processing*. McGraw-Hill, 1974.
- [46] J.-J. Xu, *Interfacial Wave Theory of Pattern Formation*. 2017.
- [47] U. Hecht, V. T. Witusiewicz, A. Drevermann, B. Böttger, and S. Rex, "Eutectic Solidification of Ternary Al-Cu-Ag Alloys: Coupled Growth of $\alpha(\text{Al})$ and Al_2Cu in Univariant Reaction," *Mater. Sci. Forum*, vol. 508, pp. 57–62, 2006.
- [48] J. L. Murray, "The aluminium-copper system," *Int. Met. Rev.*, vol. 30, no. 1, pp. 211–234, Jan. 1985.
- [49] N. Ponweiser, C. L. Lengauer, and K. Richter, "Re-investigation of phase equilibria in the system Al-Cu and structural analysis of the high-temperature phase $\eta_1\text{-Al}_1\text{-}\delta\text{Cu}$," *Intermetallics*, vol. 19, no. 11, pp. 1737–1746, Nov. 2011.
- [50] D. A. Porter and K. E. Easterling, *Phase Transformations in Metals and Alloys*. 1992.
- [51] D. M. Stefanescu, *Science and Engineering of Casting Solidification Science and Engineering*. 2002.
- [52] D. V. Alexandrov and A. P. Malygin, "Self-similar solidification of an alloy from a cooled boundary," *Int. J. Heat Mass Transf.*, vol. 49, no. 3–4, pp. 763–769, 2006.
- [53] A. Garcia and M. Prates, "Application of a Mathematical Model To Analyse Ingot Thermal Behaviour During Continuous Casting.," *IFAC Proc. Ser.*, vol. 16, no. 15, pp. 273–279, 1984.
- [54] J. Lipton, A. Garcia, and W. Heinemann, "Analytical Solution of Directional Solidification With Mushy Zone.," *Arch. fur das Eisenhüttenwes.*, vol. 53, no. 12, pp. 469–473, 1982.
- [55] "Heat Treating of Aluminum Alloys," in *ASM Handbook*, vol. 4, ASM International®, 1991, pp. 841–879.
- [56] D. Eskin and L. Katgerman, "Hardening, Annealing, and Aging," in *Handbook of Aluminum*, Marcel Dekker, Inc., 2003.
- [57] "Cobre - Propiedades del cobre." [Online]. Available: <https://elementos.org.es/cobre>. [Accessed: 20-Oct-2017].
- [58] W. Kurz and D. J. Fisher, *Fundamentals of Solidification*. Aedermannsdorf, Switzerland: Trans Tech publications, 1989.
- [59] V. S. Zolotarevsky, N. A. Belov, and M. V. Glazoff, *Casting Aluminum Alloys*. Elsevier, 2007.
- [60] P. W. Voorhees, "The Theory of Ostwald Ripening," *J. Stat. Phys.*, vol. 38, no. 1/2, pp. 231–252, 1985.
- [61] W. R. Osório, L. R. Garcia, P. R. Goulart, and A. Garcia, "Effects of eutectic modification and T4 heat treatment on mechanical properties and corrosion resistance of an Al-9 wt%Si casting alloy," *Mater. Chem. Phys.*, vol. 106, no. 2–3, pp. 343–349, 2007.
- [62] N. A. Belov, A. N. Alabin, and D. G. Eskin, "Improving the properties of cold-rolled Al-

- 6%Ni sheets by alloying and heat treatment," *Scr. Mater.*, vol. 50, no. 1, pp. 89–94, 2004.
- [63] "ImageJ." [Online]. Available: <https://imagej.nih.gov/ij/>. [Accessed: 26-Feb-2018].
- [64] X. Wei, Y. Wang, A. J. Hernández-Maldonado, and Z. Chen, "Guidelines for rational design of high-performance absorbents: A case study of zeolite adsorbents for emerging pollutants in water," *Green Energy Environ.*, vol. 2, no. 4, pp. 363–369, Oct. 2017.
- [65] S. Bhattacharyya, Y. Mastai, R. N. Panda, S. Yeon, and M. Z. Hu, "Advanced Nanoporous Materials: Synthesis, Properties, and Applications," vol. 2014, pp. 2–4, 2014.
- [66] J. A. Counter, J. Addai-Mensah, and J. Ralston, "The formation of Al(OH)₃ crystals from supersaturated sodium aluminate solutions revealed by cryovitrification-transmission electron microscopy," *Colloids Surfaces A Physicochem. Eng. Asp.*, vol. 154, no. 3, pp. 389–398, 1999.
- [67] SCHOEN R and ROBERSON CE, "Structures of Aluminum Hydroxide and Geochemical Implications," *Am. Mineral.*, vol. 55, no. 1–2, pp. 43–77, 1970.
- [68] S. Graulis *et al.*, "Crystallography Open Database - An open-access collection of crystal structures," *J. Appl. Crystallogr.*, vol. 42, no. 4, pp. 726–729, 2009.
- [69] "Match! - Phase Identification from Powder Diffraction." .

APPENDIX

Program to calculate the sample porosity through SEM images.

```
clear all
close all
clc

%% Read image
RGB = imread('SEM_image.tif');
imshow(RGB)
h = imdistline
px2um = 1/54;          % 1 um = 54 px
SIZE = size(RGB);
W = round(SIZE(1)*0.93);
RGB = imcrop(RGB,[0 0 SIZE(2) W]);
imshow(RGB)
print(gcf, 'RGBimage1', '-dpng', '-r600')
GRAY = rgb2gray(RGB);
GRAY = imadjust(RGB);
BW = ~im2bw(GRAY,0.1);
imshow(BW)
print(gcf, 'BWimage1', '-dpng', '-r600')
[B,L] = bwboundaries(BW);
figure()
hold on
```

```
for k = 1:length(B)
    boundary = B{k};
    plot(boundary(:,2), W-boundary(:,1), 'k', 'LineWidth', 1)
end
axis off
S = size(BW);
axis([0 S(2) 0 S(1)])
axis equal

figure()
imshow(label2rgb(BW))

%% AREA AND PERIMETER IDENTIFICATION
stats = regionprops(BW, 'Area', 'Perimeter');
for i = 1:length(stats)
    perimeterPX(i) = stats(i).Perimeter;
    areaPX(i) = stats(i).Area;
end
area = areaPX*(px2um^2);
perimeter = perimeterPX*px2um;
areaT = S(1)*S(2)*(px2um^2);
areaP = sum(area)/areaT
perimeterT = 2*sum(S)*px2um
perimeterP = sum(perimeter)/perimeterT

%% PERIMETER

lB = length(B);
D = 0;
for i = 1:lB
    lBi = length(B{i});
```

```
D = 0;
for j = 1:lBi-1
    if j == 1
        dx = abs( B{i}(lBi,2) - B{i}(j,2) );
        dy = abs( B{i}(lBi,1) - B{i}(j,1) );
    else
        dx = abs( B{i}(j+1,2) - B{i}(j,2) );
        dy = abs( B{i}(j+1,1) - B{i}(j,1) );
    end
    D = D + sqrt( dx^2 + dy^2 );
end
PER(i) = D;
end

%% AREA
ARE = sum(sum(BW))
ATI = S(1)*S(2);
pARE = ARE/ATI
```